REPUBLIC OF TÜRKİYE

ALTINBAŞ UNIVERSITY

Institute of Graduate Studies

Civil Engineering

CALCULATION OF HIGH CONCRETE BUILDINGS CONSISTING OF SHEAR WALL-STRUCTURAL AND FRAMES UNDER EARTHQUAKE EFFECT USING GROUP LOADING AND ETABS

Noor AL-DAFFAIE

Master's Thesis

Supervisor

Prof. Dr. Zeki HASGÜR

Istanbul, 2023

CALCULATION OF HIGH CONCRETE BUILDINGS CONSISTING OF SHEAR WALL-STRUCTURAL AND FRAMES UNDER EARTHQUAKE EFFECT USING GROUP LOADING AND ETABS

Noor AL-DAFFAIE

Civil Engineering

Master's Thesis

ALTINBAŞ UNIVERSITY

2023

The thesis titled CALCULATION OF HIGH CONCRETE BUILDINGS CONSISTING OF SHEAR WALL-STRUCTURAL AND FRAMES UNDER EARTHQUAKE EFFECT USING GROUP LOADING AND ETABS prepared by NOOR AL-DAFFAIE and submitted on 14/04/2023 has been **accepted unanimously** for the degree of Master of Science in Civil Engineering.

____

Prof. Dr. Zeki HASGÜR

Supervisor

Thesis Defense Committee Members:

Prof. Dr. Zeki HASGÜR	Department of Civil Engineering, Altınbaş University	___________________
Prof.Dr. Tuncer ÇELİK	Department of Civil Engineering, Altınbaş University	___________________
Prof. Dr. Bariş GÜNEŞ	Department of Civil Engineering, Istanbul University-Cerrahpasa	___________________

I hereby declare that this thesis meets all format and submission requirements of a Master's thesis.

Submission date of the thesis to Institute of Graduate Studies: ___/___/___

I hereby declare that all information/data presented in this graduation project has been obtained in full accordance with academic rules and ethical conduct. I also declare all unoriginal materials and conclusions have been cited in the text and all references mentioned in the Reference List have been cited in the text, and vice versa as required by the abovementioned rules and conduct.

Noor AL-DAFFAIE

Signature

ABSTRACT

CALCULATION OF HIGH CONCRETE BUILDINGS CONSISTING OF SHEAR WALL-STRUCTURAL AND FRAMES UNDER EARTHQUAKE EFFECT USING GROUP LOADING AND ETABS

AL-DAFFAIE, Noor

M.Sc., Civil Engineering, Altınbaş University,

Supervisor: Prof. Dr. Zeki HASGÜR

Date: April /2023

Pages:81

Structural Engineers are primarily responsible for determining the characteristics of a structure while exposed to lateral force, and high-rise buildings must be sufficiently stiff to withstand horizontal forces generated by storms and earthquakes. It is possible to prevent substantial displacement and, as a result, damage caused by displacement by utilizing shear walls in buildings. The previous latest damaging earthquake in Turkey was the Van 2011 earthquake, which damaged several structures, the majority of which were constructed with moment-resisting frames. This research investigates the use of shear walls over moment resisting frames at various points in a G+50 multi-story building, as well as the earthquake-exposed character of the structure using Response Spectrum Analysis. The Multi storied building was analyzed for various structural irregularity induced by the ground motion. The numerical results indicate that adding shear-wall at all the corners of the structure can be the most effective against seismic effect.

Keywords: Earthquake Damage, Response Spectrum, Shear-Wall, Story Drift, BASE Shear.

TABLE OF CONTENTS

Pages

LIST OF TABLES

<u>Pages</u>

LIST OF FIGURES

Pages

ABBREVIATIONS

SDOF	:	Single Degree of Freedom System
MDOF	:	Multiple Degree of Freedom System
LFRS	:	Lateral Force-Resisting Systems
MWFRS	:	Main Wind Force-Resisting Systems
SFRS	:	Seismic Force-Resisting Systems
RSA	:	Response Spectrum Analysis

1. INTRODUCTION

1.1 GENERAL

Braced and moment frameworks are often made of steel and otherwise reinforced concrete. Shear walls could be built utilizing numerous materials, including metal plates, reinforced masonry, timber frames containing different types of covering substance, gypsum board, drywall, internal and external plaster (stucco), plasterboard, as well as wood cladding. Shear panels, that are encased wooden panels, are employed to construct the shear walls of standard timber structures. Masonry (clay or concrete components) can be applied to create shear walls that are either reinforced or not. This section provides background information as well as an overview of the design and assessment of high-rise structure having shear walls.

1.2 BACKGROUND OF THIS STUDY

The capacity to withstand lateral loads like wind and earthquake ones and transmit those to the earth is indeed a requirement for all constructions. Several forms of force-resisting processes, including rigid frames (often known as moment frames), shear walls, braced frames, or even a hybrid of these known as dual processes, are frequently employed to withstand heavy lateral pressures throughout the perpendicular direction. This term "lateral force-resisting systems (LFRS)" is frequently used to describe those processes. Such processes are defined either Main Wind Force-Resisting Systems (MWFRS) whenever employed for wind pressure resistance; or Seismic Force-Resisting Systems (SFRS) whenever employed for seismic loads resistance.

Turkey is known as one of the most seismically active regions on the planet. Due to poor building standards, Turkey had numerous catastrophic seismic events (1992-Erzincan Earthquake, 1999-Kocaeli Earthquake, 1999-Duzce Earthquake, 2003-Bingol Earthquake and 2011-Van Earthquakes etc.) that caused numerous building collapses, destruction, as well as a significant number of fatalities. The most recent severe seismic to strike Turkey had a magnitude of 7.2 and occurred in 2011. For the 2011 Van incident, 0.18 g is the highest maximum recorded surface motion. The Van 2011 earthquake caused significant structural failure to many structures, which ranged from minor masonry partition wall cracks to complete collapses.

After the Van 2011 devastating earthquake, it was observed that RC structures suffered significant harm and perhaps fell down, with losses concentrated in the groundfloor columns directly attributed to soft stories, plastic hinges in columns [1, 2]. Substantial dislocation during earthquake is known to result in visible failure, according to earlier research. Shear wall construction minimizes structural failure through preventing significant deformations brought along by earthquake lateral forces [3, 4]. The detrimental impact of structure irregularities and shortcomings, including soft stories, short columns, inadequate confining, low design of beam-column connections, low-quality material, and so on may be eliminated by well-built shear walls for RC structures [5].

Shear walls could be considered to assure the security of the buildings against lateral forces such as earthquake ones. Walls serve as a structure's major or maybe only a component for lateral-resistance, and these structures are referred to as "shear wall buildings." It is regarded as among the most effective structural systems for mitigating lateral pressure. Shear wall-equipped RC structural systems behave well while sustaining lateral pressure as well. Numerous academics have been interested in examining overall earthquake behavior and characteristics of shear walls along with the impact of having shear walls on the seismic response. This is a fundamental issue to examine in order to gain trustworthy information regarding shear walls.

1.3 OBJECTIVES

The following are the primary goals of this investigation:

a. To investigate overall response of RC high-rise structures against lateral forces (Earthquake loads).

b. To examine how the performance of high-rise structure having shear wall varies with various location

c. To determine the shear wall's optimal placement in various situations.

1.4 ORGANIZATION OF THE THESIS

The thesis paper contains the following chapters:

Chapter 1: Introduction

This section discusses the research significance on that investigation topic. It also includes overall purpose of the investigation as well as the outline of research.

↓

Chapter 2: Literature Review

This section includes the background of this research. It describes the terms and conceptions related to this study briefly. It also shows the procedure how this research is important and how the research is processing.

↓

Chapter 3: Research Methods

This section is related with the processes and consequences adopted in the research. This section also discusses about the details of methodology which have been used in this research work. This shows various properties of the materials, analysis procedures and adopted analytical method. This section shows that how the work has been done.

↓

Chapter 4: Results and Discussion

This section shows all test findings which have been done. The necessary graphs and tables are also shown here. The explanation of these results is also described in this chapter.

↓

Chapter 5. Conclusions and Recommendations

This section includes overall outputs, decisions, and consequences. It also includes references. This also mentions advice for further studies about the topic.

2. LITERATURE REVIEW

2.1 GENERAL

This chapter includes an evaluation of earlier work and focuses on the scope of doing new & advance research. Typical shear wall types, design procedures and analysis methods that can be utilized to design shear wall are all discussed comprehensively in this chapter.

2.2 PREVIOUS STUDIES

The aim of seismic analysis is to maximize overall structural frameworks' capability during ground movement by Moment Frames [6-9], Shear-Walls [10, 11], and Braced Frames. As prediction of collapse during seismic loading has been an important component of structural engineering, experts may utilize this collapsing probability as a critical decision criteria when designing new infrastructures as well as assessing the earthquake resistance capacity of existing structures during earthquakes [12]. According to earlier research, the higher portions of the structures are the most important since they are impacted by both subsoil stiffness as well as structural vibrations [9, 13-16]. Therefore, a variety of analysis methods are employed to anticipate the destruction resulting from ground movement, including the overall infrastructure simplification to a similar single-degree-of-freedom method [17-20], the application of processive finite-element evaluation of the entire system to diagnose an enormous change in structural behaviour [19, 20] as well as suddenly established accumulative dynamic analysis [21-24]. With regard to the RC structure, the response spectrum technique particularly permits to use the response spectrum, which is characterized as a realistic illustration of peak response vs normal time for a particular accelerogram. Dynamic analysis must be performed to determine the maximum responsiveness to a baseline stimulation for a structure and also to examine its characteristics throughout ground movement [25].

Tall structures having moment frames could produce a lot of tensile and compressive pressures in the columns. Such higher tension could be particularly harmful because substantial cracks might lead to severe damage whenever the pressure is reversed as well as the component is expected to withstand twisting. Due to all this, the ACI 318-05/08 standard stipulates that the flexural strengths of columns should be minimum 20% greater than the total of the equivalent strengths of the linking beams anywhere at given story. It ensures that even if inelastic movement takes place, this will produce plastic hinges inside the beam rather than the columns. According to the assessment of B. Shafei, F. Zareian, and D. G. Lignos [12], moment-resistant frameworks are sufficiently capable of preventing the breakdown of Reinforced structures which are subjected to ground shaking. Additionally, Seo et al. [26] & S. Akhil Ahamad [25] recommend adding a Shear-Wall using Moment Resistant Framing to manage the deflection and drifting of a RC building.

Coull and Wong [27] discussed the impact of local elastic wall deflections upon those interactions of slabs with flanged shear walls. The contact among floor slabs and laterally loaded flanged shear walls in crossing wall systems was investigated using a finite element approach. Considerable focus was placed over how local elastic wall deflections affected the coupling stiffness, slab's effective width, as well as critical bending moments. In order to forecast how inelastic RC structure having shear wall will respond to earthquakes, encompassing flexural as well as shear 16 modes of failure, Hidalgo, et al. [28] constructed an analytical model. The most common type of failure within RC shear walls is flexural mode. However, there are certain instances when this ductile failure might not be realized because of the walls' high flexural strength relative to their strength properties. Such circumstances are likely to result in to an undesirable shear failure scenario.

Tasnimi [29] developed four one-eight sized shear wall concepts that used cyclical shifting forces as well as an ACI-recommended configuration. All of the models had the same materials, dimensions, and reinforcements; the only difference was the cyclic loadings. Utilizing load deflection charts, the test report's findings were contrasted with the ACI standards.

Satpute and Kulkarni [4] established a numerical model to investigate the earthquake behaviors of a ten-story RC shear wall building both with and without openings. It then used nonlinear techniques including pushover method and time history to examine this RC shear wall building. The analysis was done employing SAP 2000. For the construction of RC shear walls containing and without openings, story drift as well as base shear was contrasted.

Burak and Comlekoglu [30] carried out an experimental investigation to assess the impact of the shear wall/floor space ratio upon that seismic response of medium - rise RC constructions. The findings suggest that in order to manage drift, medium - rise structures must be designed with shear walls that have a shear wall ratio of a minimum of 1%. A shear wall proportion exceeding 1.5 percent, a boost in seismic behavior is not sufficiently considerable.

Dashti, et al. [31] Dashti looked into how a conventional wall constructed in accordance with various standards performed during earthquakes. With respect to its bending, lateral load capacity, as well as displacement ductility, the walls' nonlinear reactions were analyzed.

Heerema, et al. [32] evaluated a two-story RC building until collapse while using completely inverted quasi-static displacement regulation. The structure's lateral load-resistance structure is made up approximately eight walls. A core of stiffness eccentricity from the flooring mass centers with about 20% of structure width was achieved by placing four walls irregularly, as well as the remaining 4 walls were positioned uniformly all-around flooring mass centers in order to give torsional restrictions. They found that when assessing an entire building earthquake pressure resistance mechanism, it is important to take into account the strength of the wall contributing to entire structure capacity, variations in the inelastic performance parameters of the various walls that make up the structure's earthquake force-resisting scheme, as well as the resultantly mobilized ductility rates.

El-Azizy, et al. [33] looked at the seismic behavior of RC walls utilizing various cross-sectional arrangements and vertical reinforcement ratios. Three distinct cross - section arrangements of the walls—rectangular, flanged, and boundary elements—were investigated using quasi-static deformation regulated cyclic loading. According to the investigation, incorporating flanges as well as boundary components walls allowed for a 30% decrease in vertical reinforcement as contrasted with rectangular walls whenever designed to withstand similar lateral pressure and transport the same loads. Additionally, they suggested that structural walls featuring lower vertical reinforcement ratios would have less ductility.

In accordance with FEMA guidelines, Seo, et al. [26] investigated overall earthquake resistance of a 12-storied RC moment-resisting structural frame including shear wall. Responsive spectrum analysis as well as nonlinear time history analysis methods were used to evaluate effectiveness. This research found that as height increased, floor-level vulnerability generally decreased for overall FEMA performance, and also the proportions from both techniques largely complied with the established restrictions.

Gogus and Wallace [34] looked into the RC walls' Deflection Amplification Factor, Response Modification Coefficient, including Systemic Overstrength Aspect. To verify those characteristics, 20 special and 20 regular RC walls were developed under various earthquake design situations. Except for the templates possessing height-to-length proportions approaching 3 or larger, the results showed that the attributes of the templates created utilizing the current standard specifications are all within acceptable parameters.

An research work upon RC walls with little restricting reinforcements than that advised by ACI 318 [35] was conducted by Li et al. [36]. Additionally, strut and tie prototypes are created to aid in comprehending the pressure transmission inside the evaluated walls.

Khanmohammadi and Heydari [37] studied at the seismic response of the base-rocking mechanism involving shear walls, metal brace frames, and prefabricated modular bridge piers. As a result, various shear wall structures were examined. They stated that the drifting proportions were comparable to the base rocking system's outcomes and don't grow roughly compared to the standard wall's finding.

Jalali and Dashti [38] investigated how well a straightforward macroscopic system could foresee overall nonlinear behavior of thin reinforced concrete shear walls. ABAQUS 6.6 was used to carry out the investigations. They examined the outcomes of analytical and empirical testing samples and found that there was considerable harmony with the samples' empirical observations.

A computational evaluation of shear wall constructions as well as frame structures containing shear walls was conducted by Aktaş [39]. The same prerequisites were used to create each of the structures under consideration. In a parametric analysis, 317 distinct buildings' deformation-displacement relationships were provided based on the shear wall percentage.

Sanni-Anibire, et al. [40] researched the nonlinear behavior of intermediate aspect ratio shear walls involving cyclic and monotonic loads and according to them, shear walls are the safest alternative for resisting lateral pressure in multi - storied RC structures

Assuring that structures meet specific quality standards (such as minimal damage, considerable harm, and collapse mitigation) while subjected to a seismic attack is a crucial aspect of high-rise building designs. Different earthquake design and assessment methodologies were created to overcome this problem. It is hard to foresee the magnitude and timing of upcoming disasters, despite seismology's ongoing advancements. The use of probabilistic approaches in the evaluation and planning procedure is essential because of the earthquake's unpredictable character. One of these statistical models is performance assessment through dynamic analysis including fragility assessment, that demonstrates the best structural functionality during earthquake loading in addition to the probability of going above a specific damage level. That style of dynamic analysis has been utilized to assess the earthquake vulnerability of structures composed of various building materials. Because of the perceived significance attached to this type of structure, numerous investigators who implemented similar approach to high-rise RC structures concentrated on those with more than 30 floors. To illustrate, Applying linear dynamic simulation with nonlinear time history assessment, Ji et al. [41] established the analytical behavior of a 54-story RC structure. Alwaeli, et al. [42] used incremental dynamic analysis (IDA) to produce fragility curves for a30-storied RC structural model. Değer, et al. [43]; Değer and Wallace [44] investigated the seismic behavior of a 42-storied reinforced concrete structure with several structural components, comprising core wall buildings equipped with and without MRF as well as a duel-system developed utilizing two separate methodologies. Employing IDA tools, Aman, et al. [45] evaluated the comparative earthquake effectiveness of five 60-storied reinforced concrete structures of various concrete strengths. It was determined that high-strength concrete not only reduces building costs but also behave seismically more safely than conventional concrete strength at higher ground movement intensity ranges. Despite the fact that mid- to tall structures are crucial to research, their prevalence is typically smaller than that of regular structures, which are frequently utilized like homes. There is a critical necessity to investigate the earthquake resistance of lower high-rise structures employing dynamic analysis since the collapse and fall of these high-rise structures will have an immediate effect on the lives of millions of occupants.

There are numerous academic papers regarding shear wall structures' earthquake sensitivity. However, only few of them covered the connection among shear wall designs and earthquake behavior of structures. In order to evaluate actual optimum top story deformations, Firoozabad, et al. [46] performed a linear time history study using structures containing six different shear wall layouts that had been subjected to two actual seismic events. It was discovered that stronger seismic activity would not necessarily result from larger shear barriers. Chandiwala [47] compared the base shear pressures of the five shear wall places within an identical L-shaped high-rise (random arrangement in plan) and came to the conclusion that for L-shaped construction drawings, the shear wall at the extreme ended up giving the greatest result through immediately impeding terminal oscillation throughout earthquakes as well as lowering bending moment of the high-rise. Sardar and Karadi [48] analyzed the ELF and response spectrum of five 25-story structures having identical layout and five different shear walls arrangements. Structures with L-shaped shear walls around extremities including core shear walls produced minimal base shear, as shown by evaluating respective story shear forces, drifts, as well as shear deformations. Three high-rise RC buildings with varying numbers of shear walls and an identical Y-shaped structure were constructed and assessed by Kim, et al. [49]. The structure with the greatest number of shear walls seemed to have the greatest strength and offered the greatest spatial variability freedom, even though additional resources were needed, according to the IDA and nonlinear static pushover analysis.

2.3 SHEAR-WALL AND LOAD PATH OF A SHEAR-WALL

A wall that is intended to withstand lateral forces adjacent towards the wall's plane is known as a shear wall. In-plane pressures are indeed the name given to such pressures. Based on its ultimate use, a shear wall can be either a load- carrying wall or even a non-load-carrying wall. It would qualify as a load-carrying wall if it needed to withstand lateral loads as well as gravitational forces from the supporting components (like the ceiling or flooring). A shear wall resists in-plane pressures through virtue of its strength under shear, as the title suggests. The wall's cross-sectional region which withstands shear is calculated by multiplying its height by thickness. Gravitational and lateral forces impacting on a shear wall are seen in Figure 2.1.

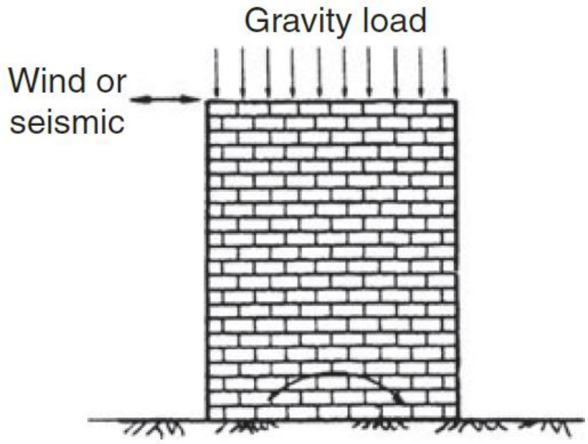

Figure 2.1: Gravity and Lateral Loads on A Shear Wall.

Understanding the lateral forces pathway in structures containing shear walls is essential. Shear walls serve as the LFRS in these structures. They primarily take their pressures from either the ceiling or flooring that they are supporting. Bearing transfers gravitational pressures from the roof or floors to the shear walls. Utilizing linkages between both the supporting components that serve as diaphragms and the shear walls, lateral forces are transmitted through the same supporting components as inertial forces. As a result, the floors as well as the shear walls work together as a group of structural components to withstand horizontal and gravitational pressures.

Diaphragm pressures are the inertial loads produced in the floor and roof that are aligned throughout the horizontal pressure resistance plane components. Diaphragms are horizontally force-resisting components that work to transmit lateral pressure towards the vertical supports and are typically either floors or ceilings of structures. It functions fundamentally as a huge beam that is horizontal. Shear walls, that function like perpendicular cantilevers and transmit those pressures to the soil surface, receive the inertial loads from the diaphragms (Figs. 2.2 to 2.3).

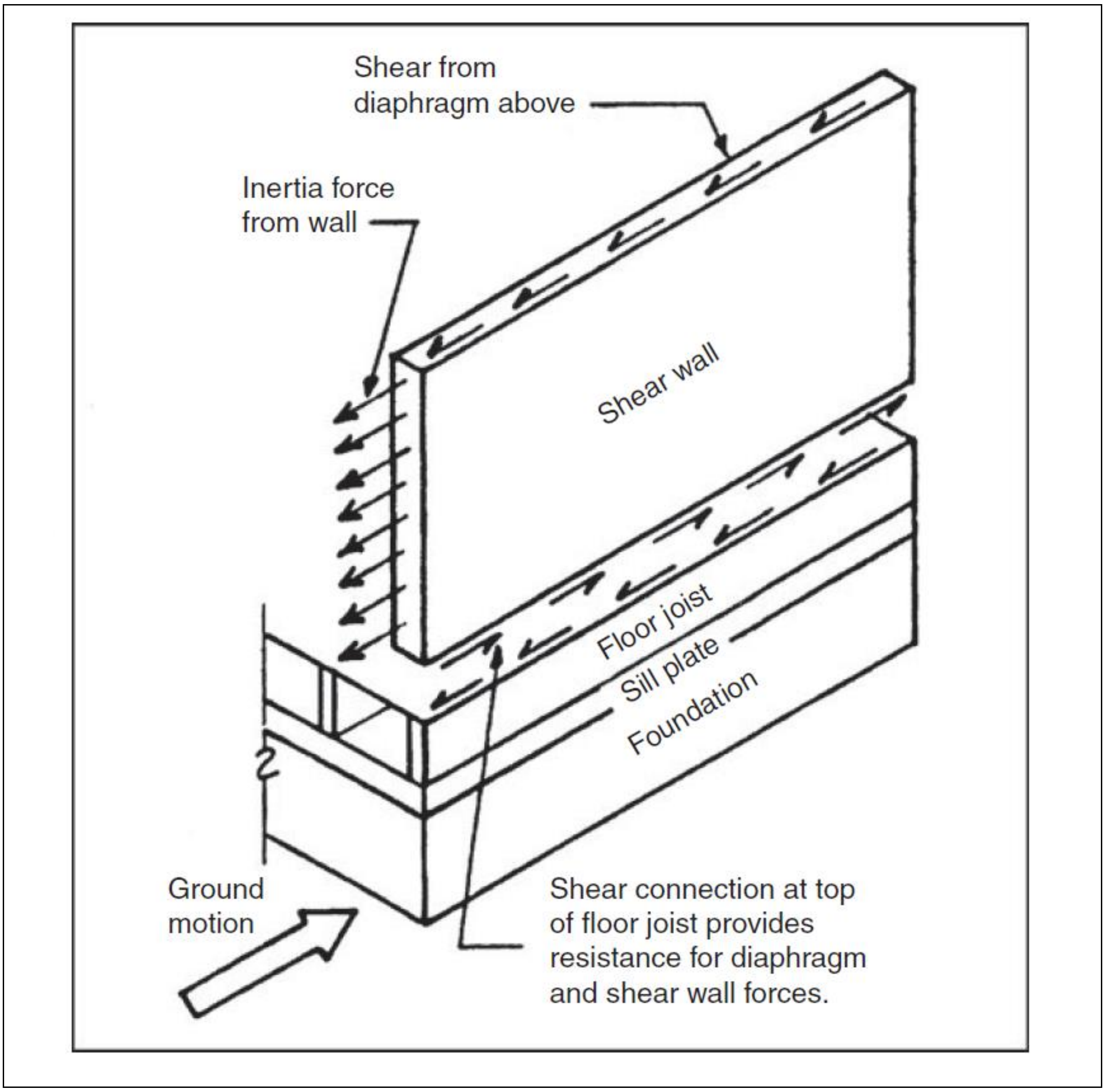

Figure 2.2: Inertial Forces and Resistance of Walls Parallel To Direction of Ground Motion.

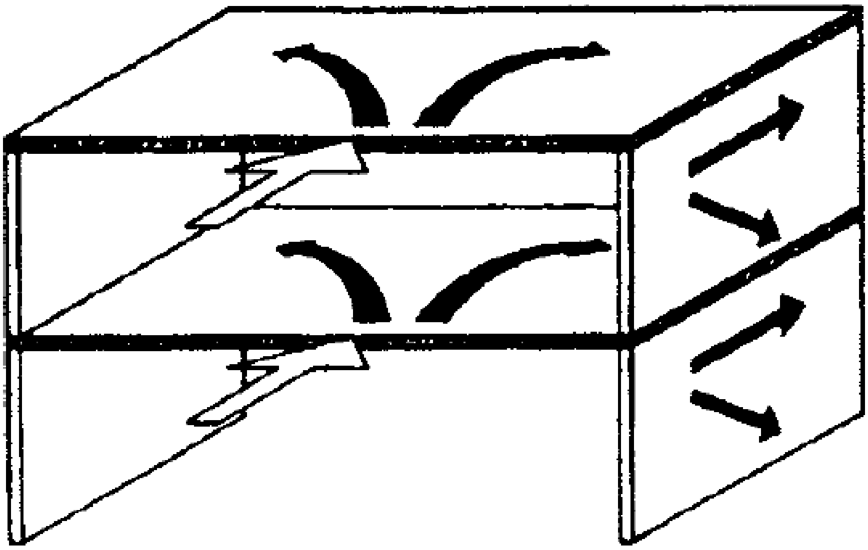

Figure 2.3: Load Path in a Shear Wall Building.

A shear wall's stiffness determines how well it can withstand lateral loads. The shear wall’s aspect ratio is expressed as the proportion of its height to length, or h/d which determines how stiff it is; the smaller its h/d proportion, the stiffer the shear wall. A shear wall behaves as a large vertical cantilevered when confronted with lateral pressures as well as being liable to both shear and flexure. The shear wall lengths are comparable to the cantilever beams’ depths, but the height of a shear wall is comparable to its length. The shear wall’s stiffness increases with length for a specified height. The link between the stiffness and ratio of shear walls is depicted in Figure 2.4. Reduced h/d proportion walls, often known as squat walls, function as shear components, exhibiting shear-related deformation predominating. Squat walls having h/d proportions between 2 and 3 are frequently used in low-rise structures.

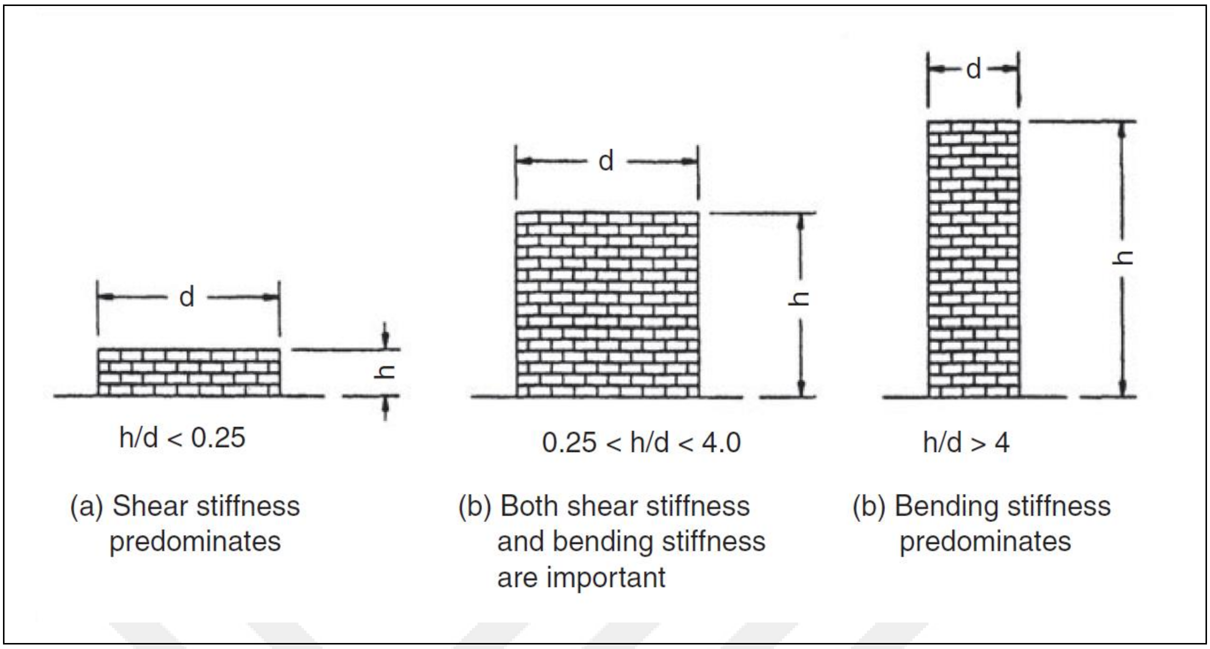

Figure 2.4: Aspect Ratio and Stiffness of Shear Walls.

It should be remembered that such walls should have sufficient strength to withstand the aforementioned pressures in order to function as bearing wall components:

a. gravitational pressures that may be imposed eccentrically on diaphragms (floors or ceilings).

b. lateral or in-plane forces that the diaphragms have applied.

c. out-of-plane pressures that are operating transverse to it as a result of wind or an earthquake.

2.4 SHEAR-WALL TYPES

Shear walls could be categorized in a number of ways based on the scope. Based on whether they additionally bear gravity loads along with lateral forces, they can be categorized as load-carrying or non-load-carrying wall. They can be selected depending upon that brickwork and constructing methods employed, such as bricks or concrete, single or multiple wythe, reinforcing or unreinforced, solid or perforated, cantilever or linked, single story or multistory, rectangular or flanged, etc. Shear walls with a rectangular or flanged design are the most popular. Fig. 2.5 displays a variety of shear wall forms.

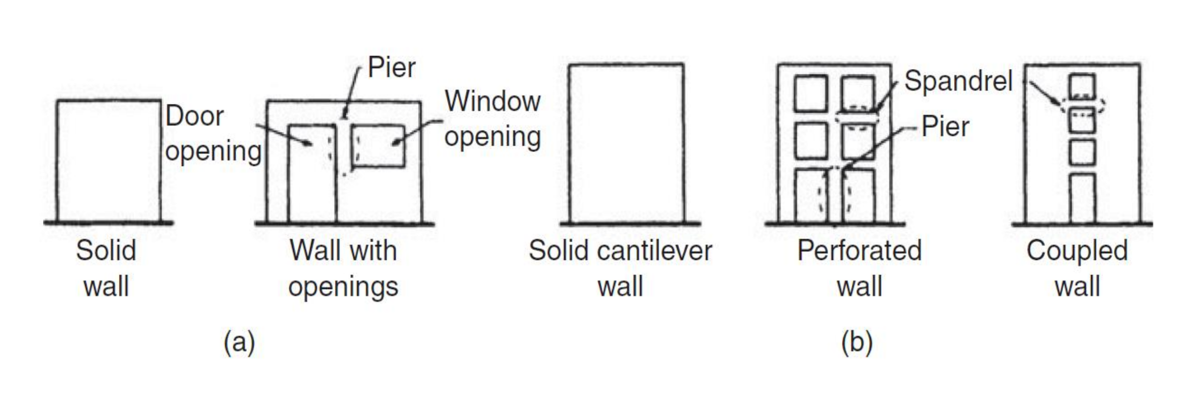

Figure 2.5: Types of Shear Walls: (a) Single Story, (b) Multistory.

The rigidities of shear walls provide the greatest description of its effectiveness. Strong shear walls are consequently the most effective and thus greatly desired. As a consequence of necessary measure, shear walls frequently contain gaps in those like be windows and doors; these walls are often considered as perforated that means a wall having openings. A shear wall's section above the neighboring entries is referred to as a spandrel or a beam, whilst the section of a wall within two adjoining spaces is known as a pier. It is possible to think of a shear wall containing apertures as a frame made of small, stiff wall sections which is also known as piers. For practical reasons, numerous shear walls must have a consistent pattern including openings, doorways, or perhaps both. In these kinds of circumstances, spandrels could be employed to link the walls between apertures, creating linked shear walls. In order to transmit shear through one wall section to the next, the joining components (i.e., beams) among connected shear walls often need both vertical and horizontal strengthening (Fig. 2.6). The walls are considered as noncoupled and may be understood as cantilevers anchored at the foundation whenever the linking pieces are unable to transmit shear through one wall to another.

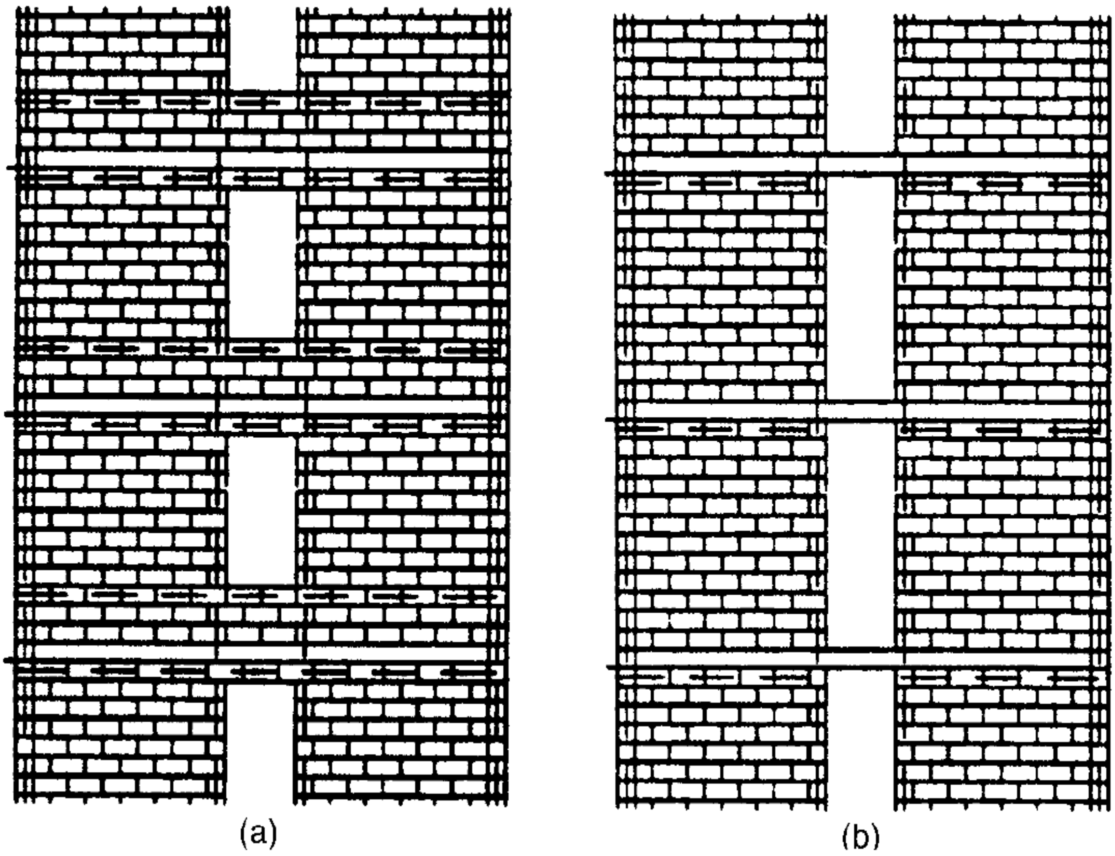

Figure 2.6: (a) Coupled and (b) Noncoupled Shear Walls.

In order to create exceptionally structurally efficient solutions, ideally suited towards ductile reaction with really excellent energy dissipation properties, gaps in shear walls could be created in a systematic as well as logical design. But shear walls become less rigid when there are apertures. Fig. 2.7 illustrates how apertures affect coupled shear walls.

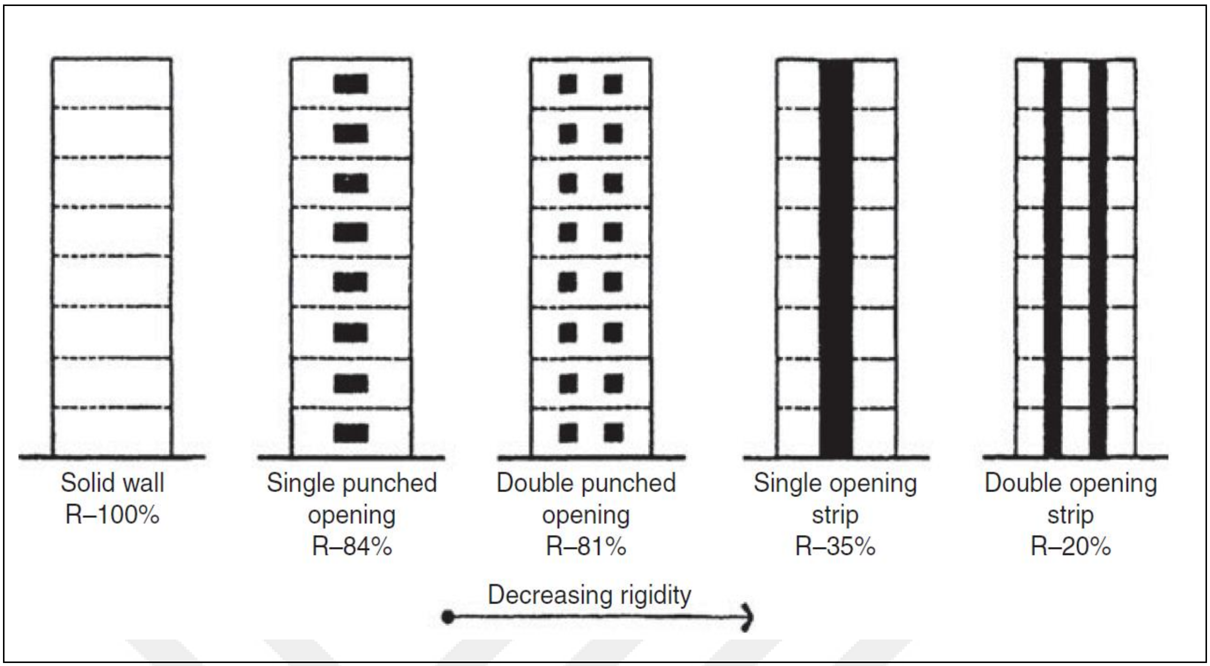

Figure 2.7: Rigidity Effects on Opening.

Flanged arrangements are created when shear walls intersect around right angles, and all these arrangements are known as flanged walls. In these circumstances, a part of the intersected wall may indeed be regarded as shear wall's flange like a T-section or an I-section. These walls are typically needed to withstand seismic loads coming from the structure's two main directions. In Fig. 2.8a, various flanged arrangements are depicted. The amount of the flange's width that ought to be taken into account for effectiveness must be determined by the engineer. An observational criterion for the flange's effective width sets the least of the following as the width that can be regarded sufficient upon every aspect of the web:

a. The genuine flange that runs along the web wall on each side.

b. a thickness that is six times the nominal value whenever the flange is compressed (Fig. 2.8b).

The effective flange width cannot exceed beyond a moving connection along with the restrictions listed previously. The effective flange width should not be added to the region of shear wall utilized throughout the horizontal shear measurement.

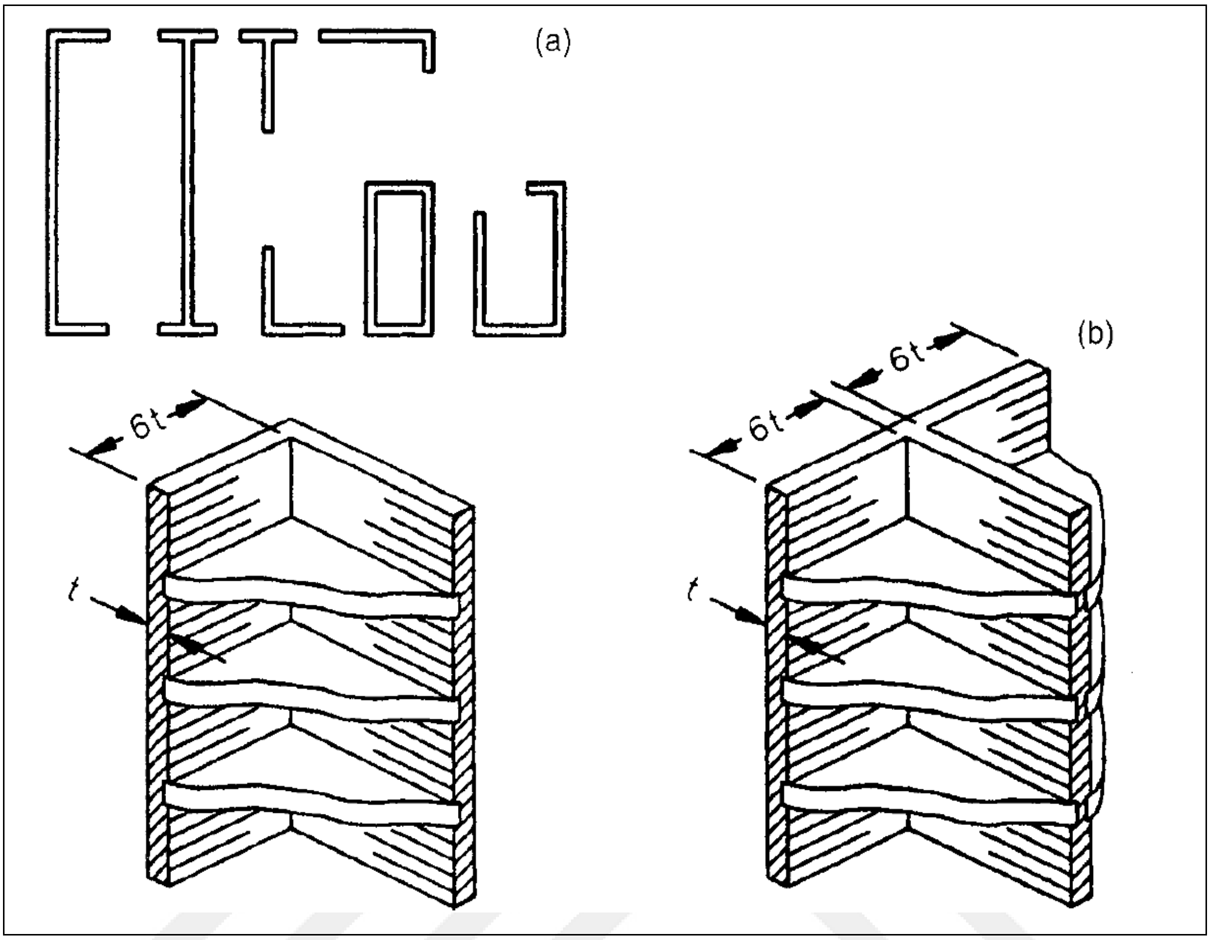

Figure 2.8: Sections of The Walls: (a) Wall Configurations Section, (b) Considering Effective Depth.

The two converging walls should be sufficiently connected at the crossing for a shear wall to function as a flanged component. Bond beams, steel anchor, running bonding can be used to attach the webs to the flanges of shear walls. Running-bond configuration must have "T" shape across its shared crossover, as illustrated in Fig. 2.9. As a replacement, steel anchors like those in Fig. 2.10 or bonded beams like those in Fig. 2.11 could be offered. The detailing that may be employed to avoid bonds between the two overlapping walls is also depicted in Fig. 2.11.

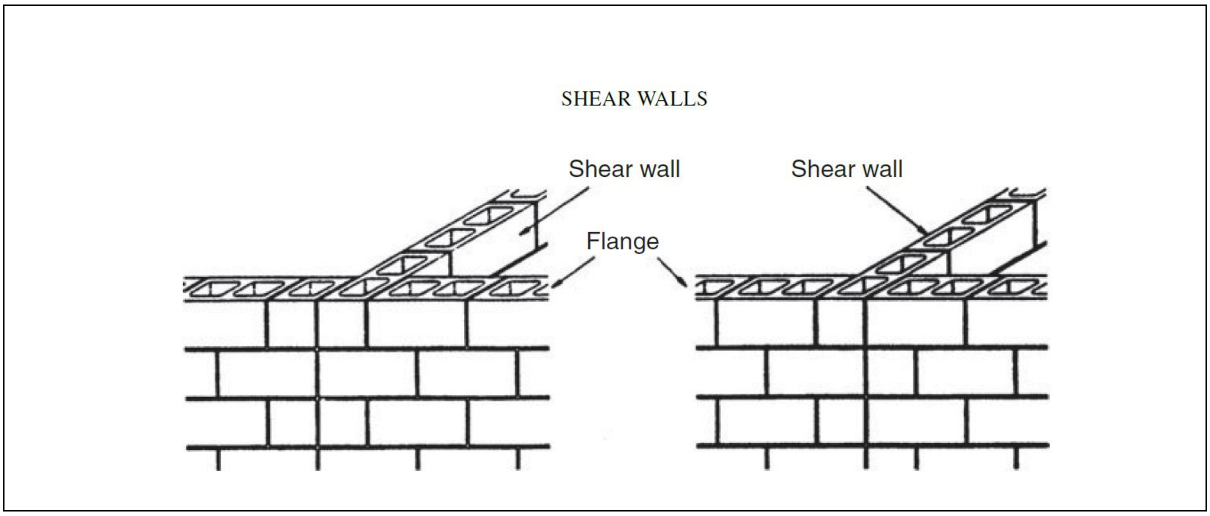

Figure 2.9: Running-Bond Lap at Intersecting Walls.

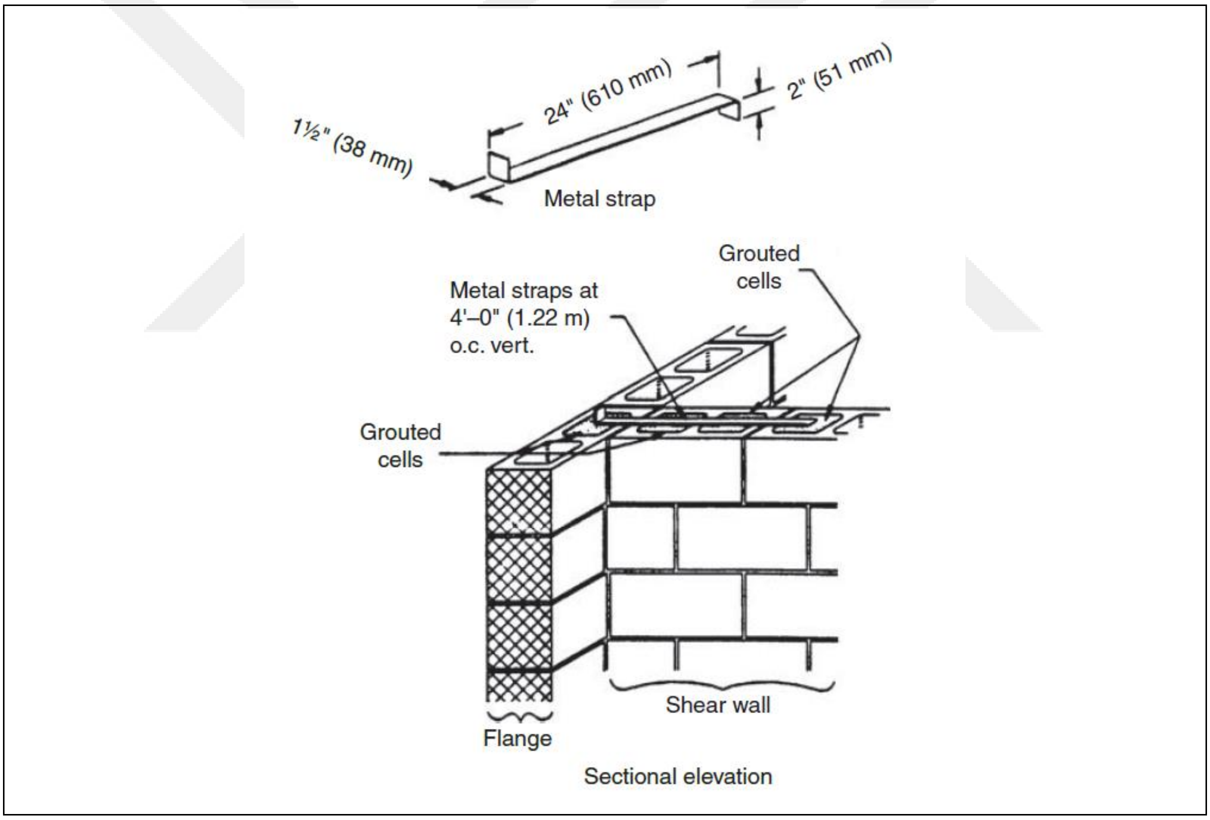

Figure 2.10: Metal Straps and Grouting at Wall Intersections.

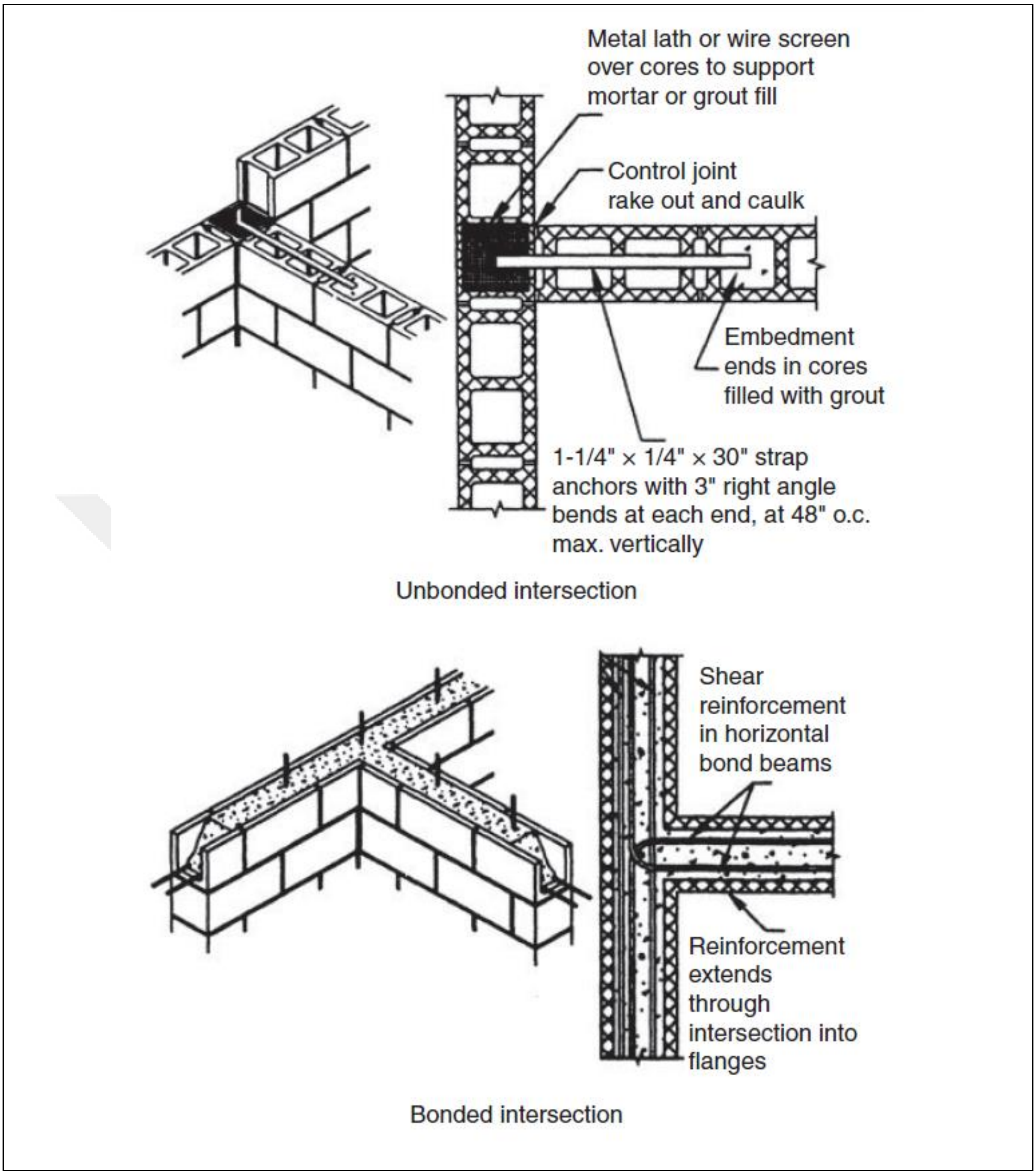

Figure 2.11: Reinforcement in Bond Beams at Wall Intersections.

2.5 EARTHQUAKE

Whenever the gravity or elastic stability of the rocks beneath or on the earth's surface is momentarily disturbed, this results in vibrations or oscillations of the ground surface, which we know as earthquakes. Elastic impulses or waves are created by the disruption and the resulting motions. Based on the nature of the forces that trigger them, natural earthquakes can be categorized as tectonic (involving the plate’s relative motion), plutonic (involving modifications at a deeper level), or volcanic.

2.5.1 Elastic Rebound Theory

According to the elastic rebound hypothesis, tectonic earthquakes occur when a region's strain accumulates over time, leading to an increase in the quantity of elastic forces stored and eventually triggering an earthquake. As we've already established, continental drift is caused by the collision of newly developed oceanic plates with the older, more stable continental plates. Frictional resistance at the plate borders may lock the plates in place at the collision site, preventing movement. This results in strain energy being stored along the plate boundaries until they suddenly slide owing to rock fracture or elastic rebound, potentially causing the earth's top crust splitting across a given path and forming a fracture. An earthquake's cause lies here. Elastic rebound is a term used to describe the slow buildup and eventual release of tension and strain. The elastic rebound hypothesis proposes that earthquakes are caused by the rapid movement of ground on either side of a fault as a consequence of the rupture of crustal rock. Extreme rigidity and strength characterize the higher reaches of Earth's crust and lithosphere. Deformation causes a very small bending in this rock (Fig. 2.12). Still, it's flexible enough to endure little pressure or bending without breaking. According to the elastic rebound hypothesis, the strain must quickly increase until it reaches the rock's elastic limit. After this point, a fault forms in the earth's crust, and the deformed rock regains its former shape, discharging all energy trapped inside as rebound and jarring vibrations (elastic waves). The earth is shaken by these vibrations, especially in the zone of the fault. Following an earthquake, strain will once again accumulate at this altered rock contact. Interpolate earthquakes are the most common type of seismic that happen across tectonic plate borders. Others are known as intraplate earthquakes because they take place inside of the plates itself, far from of the boundaries. In both forms, slips are produced at the fault during the earthquakes inside the horizontally, vertically, and lateral dimensions, designated as dip slip [Fig. 2.12(a)] and strike slip [Fig. 2.12(b)], respectively.

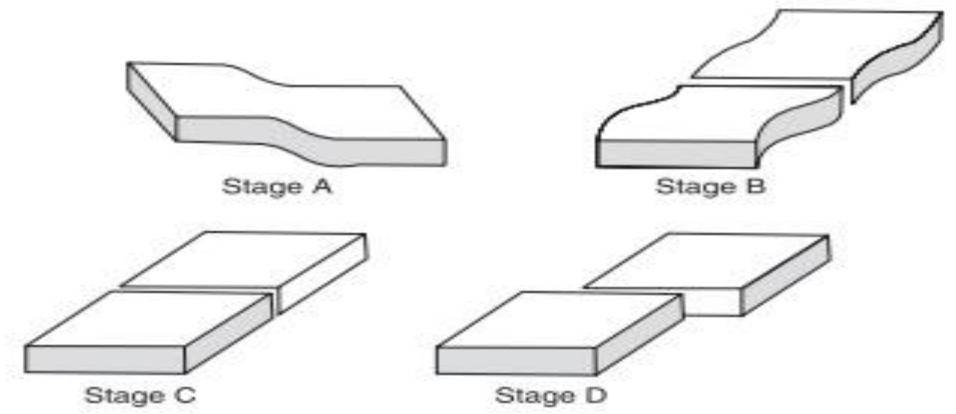

Figure 2.12: Step A: Gradual rock Deformation Step B: Rupture Stages Step C: Gaining the Original Form Step D: After Earthquake Happen.

2.5.2 Plate Tectonic Theory

The concept of plate tectonics has emerged as a result of research into phenomena including continental movement, volcanic activity, and ocean bottom ridges. Large, hard blocks, or crustal plates, make up the earth's crust, so the theory goes. These plates, which may carry land masses, oceans, or both, are in a continual state of motion on the sluggish mantle, riding atop, diving under, clashing with, or even brushing against one another. However, there are certain sections of neighboring plates that stay immobile stuck together for extended periods of time before suddenly breaking free (faulting) and causing seismic waves across boundaries which wreak havoc [50]. Continental drift where the two plates are moving away from each other, hilly building due to slower forward plate colliding with the faster back plate, volcanic eruptions, and earthquakes are all results of plate tectonics. Also, the plates might move in tandem in one way or in two distinct ways. As crustal plates move in relation to one another, they create three distinct plate borders. Fig. 2.13 depicts the three distinct kinds of plate boundaries: transform (conservative margin), convergent (destructive margin), divergent (constructive margin), or parallel [51].

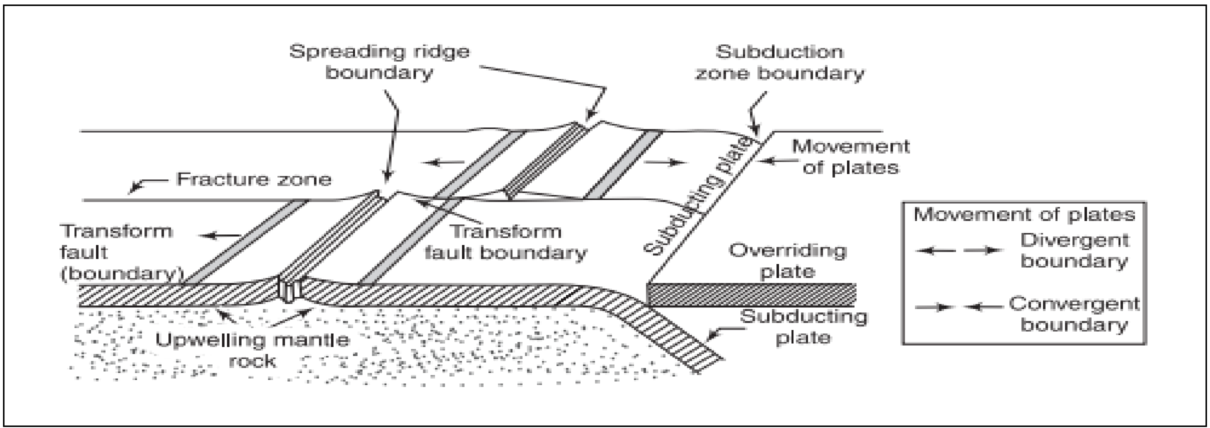

Figure 2.13: Types of Plate Boundaries.

2.6 BEHAVIOURS OF SHEAR WALL UNDER SEISMIC LOADING

Shear walls may act as tall and thin walls, short and stocky walls, or any hybrid of the two. The height to breadth proportion of typical shear walls is 2. The way they act is similar to a vertical cantilever beam. Since bending is so important in deformation, shear deformation may be ignored. Squat shear walls have a height-to-width proportion below 0.5. The shear deformation of these walls is much greater than the bending deformations. As a result, shear strength is the determining factor for these sorts of walls. The thin wall is regulated by flexural strength. The ideal shear wall response is ductile. Shear walls in RC structures that have been appropriately built have performed exceptionally well during previous earthquakes [52].

3. METHODOLOGY

3.1 VARIOUS STRUCTURAL IRREGULARITIES AND THEIR LIMITS

3.1.1 Story Stiffness

When an earthquake hits, the weakest areas in a structure are the first to give way. This fragility is caused by a break in the mass, rigidity, and form of the structure. Structures with interruptions in their continuity are said to have an irregular form. An example of structural irregularities is shown in Figure 3.1.

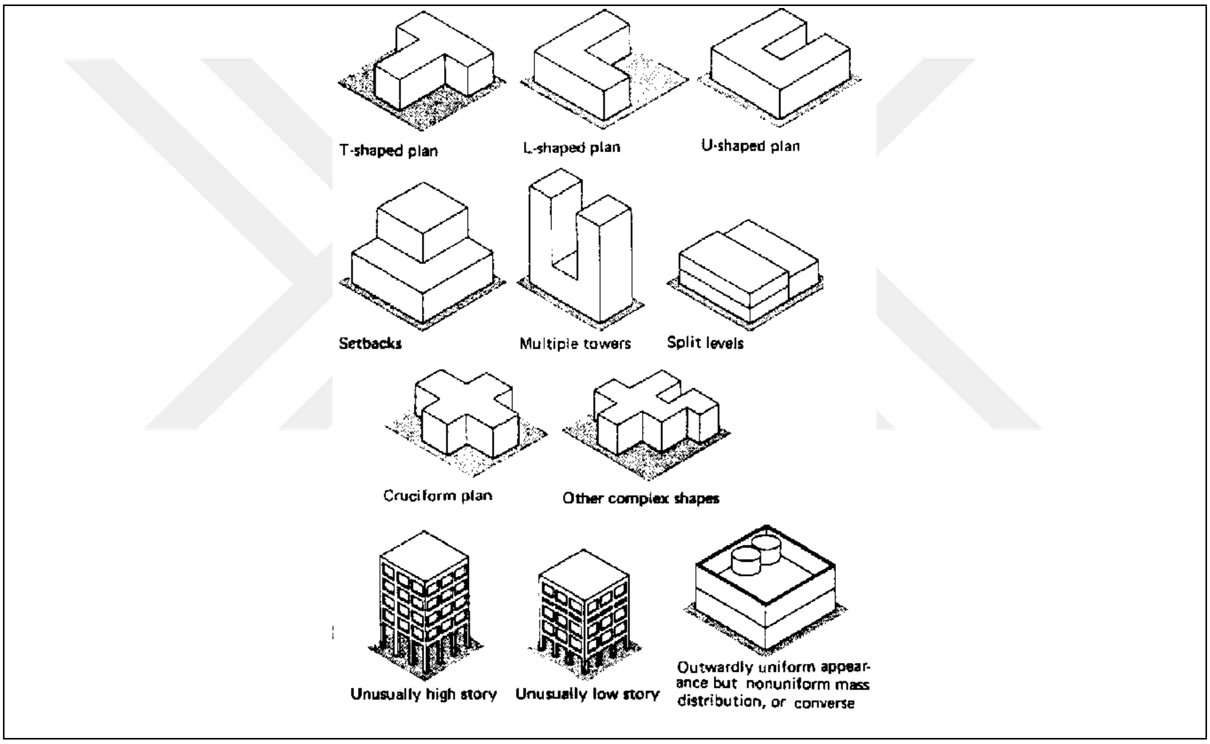

Figure 3.1: Story Irregularities.

3.1.2 Horizontal Irregularity (Soft Story)

It is present if the stiffness of a floor is less than 70 % also, it is present if the above three floor stiffness is gained not more than 80%.

3.1.3 Horizontal Irregularity (Extreme Soft Story):

To meet the criteria for its existence, a story's lateral stiffness must be either below 60% compared to the level beneath as well as 70% less than both the mean stiffness.

3.1.4 Weight (Mass) Irregularity

It is stated to be present in a site if the effective weight of one story exceeds 150 percent of the effective index of one of the stories next to it. It is not required to take into account a roof that is thinner than the floor underneath it. Figure 3.2 depicts a structural irregularity.

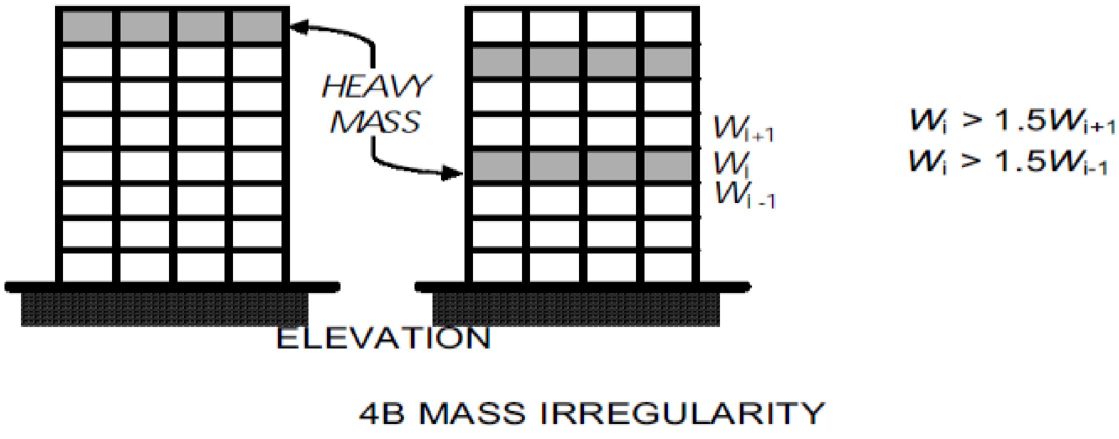

Figure 3.2: Mass-irregularities.

3.1.5 Story Displacement

The seismic displacement under strength-level design earthquake loads is the actual horizontal deformation of any position in the structure relative to its base. Figure 3.3 is an example of tale displacement.

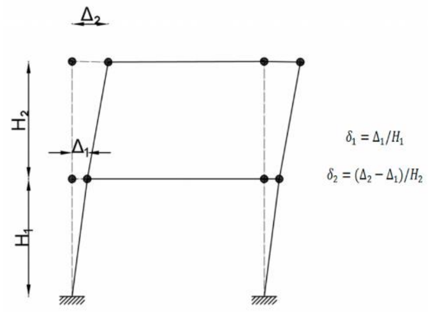

Figure 3.3: Story Displacement.

3.1.6 Drift

Story drift is the lateral displacement of a floor in proportion to the floor below, and the story drift ratio is computed by dividing the amount of story drift by the overall height of the structure. Figure 3.4 is an example of tale drift.

Figure 3.4 shows how to calculate "story drift," which is defined as the "relative elastic displacement" of one narrative in respect to the one underneath it. The points granted for this comparison, on the other hand, will vary based on the following:

a) For a structure with aligned centers of mass, the narrative drift may be determined by examining the deformations of the cores of mass.

b) The drift of a building in which the centers of mass are not aligned may be calculated by making a vertical forecast from the higher story's mass center to the lower story's mass center and then utilizing the projected point's deflection.

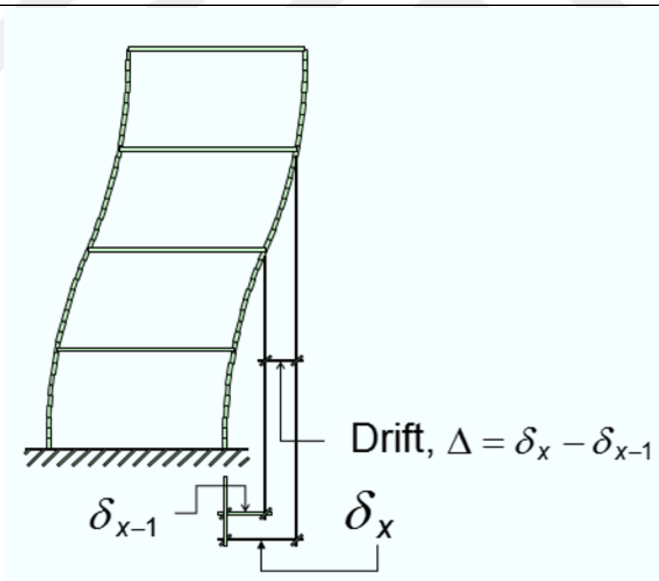

Figure 3.4: Story Drift.

The Design Δ, drift, denoted by the symbol, is determined by subtracting the Design Seismic Deflections, denoted by the symbol δ_D, at the centers of mass situated at the top or bottom of the stories that is being taken into account. It is permissible to calculate the displacement at the bottom of the tale depending on the vertical projection of the mass's center at the top of the story in cases when the centers of mass do not line vertically.

When calculating the design story drift, it is possible to ignore the effects of diaphragm deformation. The rotation of the diaphragm is to be considered in the following manner. For buildings that are classified as Seismic Category C, D, E, or F and feature horizontal irregularity, the design story drift, denoted by the symbol, must be calculated using the biggest difference between the design earthquake and the actual earthquake. repositioning of collinear points located at the top and bottom of the Δ under examination along any of the sides of the building, taking into account the consequences of diaphragm rotation. Table 3.1 outlines the allowable amount of story drift in accordance with ASCE 7-22.

Table 3.1: Allowable Story Drifts.

Structure type	**Risk Category**		
	I or II	**III**	**IV**
Structures that are not masonry shear wall structures and that are fewer than four stories above the foundation and have internal walls, divisions, and ceilings that have been constructed to accommodate the drift associated with the Design Earthquake Displacements are considered to be seismically resistant.	0.025h	0.020h	0.015h
Structures made of masonry with cantilever shear walls	0.010h	0.010h	0.010h
Other constructions that use masonry shear walls	0.007h	0.007h	0.007h
Every other type of buildings	0.020h	0.015h	0.010h

3.1.7 Base Shear

Base shear is an estimate of the largest predicted lateral force acting on the base of the structure as a result of seismic activity. This force acts laterally and causes the structure to move laterally. For the purpose of computing it, the seismic zone, the soil material, and the equations for lateral force taken from the building code are utilized (Figure 3.5)

The base shear of a structure, denoted by V, in a certain direction needs to be computed using the following equation:

$$V = C_s W \tag{3.1}$$

Here,Response coefficient, denoted by the symbol Cs,

W = The Actual Seismic Weight for Each Section

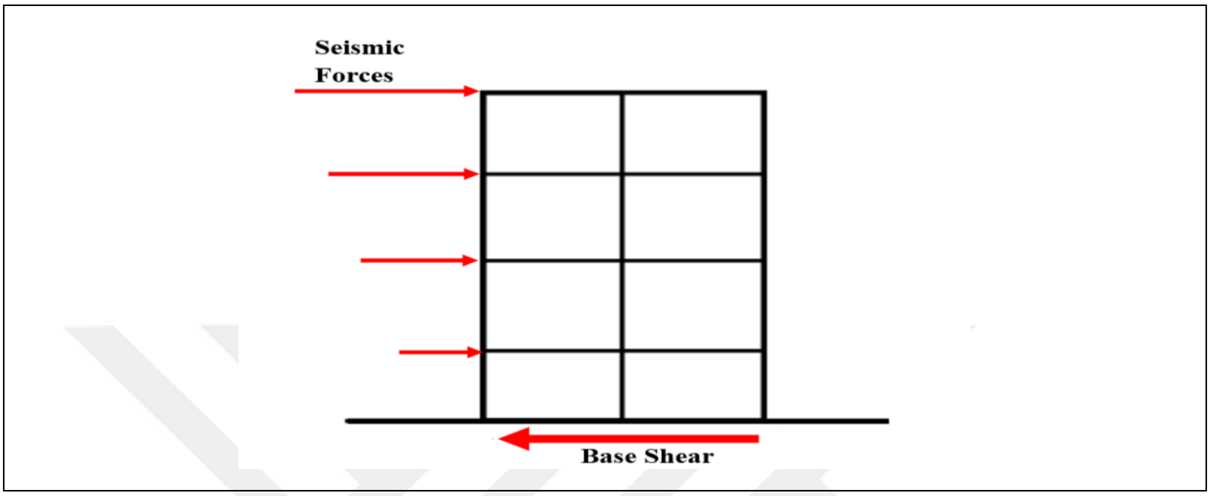

Figure 3.5: Base Shear.

3.1.8 Factor of Importance

It is required that each structure be given an Importance Factor, denoted by Ie, and discussed in Table 3.2.

Table 3.2:. The Flooding, Storm, Tornado, Snowfall, Quake, and Ice Load Categories are Assigned to Structures and Buildings According to Their Risk.

Use purpose	Category of Risk
In the event of their collapse, buildings which pose a minimal threat to human life are considered safe.	I
Every building, with the exception of those that are designated in Risk Types I, III, and IV	II
Types of buildings, the collapse of which could represent a significant threat to human life	III
The term "essential facilities" can be applied to a variety of different types of buildings.	IV

Table 3.3: *Ie* Factor Based on Table 3.2 .

Category of Risk	***Ie***
I	1
II	1
III	1.25
IV	1.5

3.1.9 Torsional Irregularity

When the maximum story drift, calculated taking unintentional torsion into account, occurs during one end of the building transverse to an axis and is larger than 1.2 times that average of the story drifts at the opposite edges of the structure, torsional irregularity is present. This is the definition of torsional irregularity. Only buildings with rigid or semi-rigid diaphragms are subject to the criteria for torsional irregularity in their structures.

3.1.10 Extreme Torsional Irregularity

Extreme torsional irregularity is defined as existing when the highest story drift, calculated which include accidental torsion, at one end of the building transverse to such an axis is larger than 1.4 times the mean of the story drifts somewhere at two ends of the structure. This definition applies only when the maximum story drift is measured at one end of the structure. Only structures with rigid or semirigid diaphragms are capable of having extreme torsional irregularities.

3.2 THE RESPONSE COEFFICIENT CALCULATION

Method 1 or Method 2 may be used to calculate the seismic response coefficient, Cs, in situations in which the original spectral acceleration variable Sa was computed in line with either Chapter 11.4.5.1 (ASCE 7-22). Method 1 and Method 2 must both adhere to the lower bound specified for the linear dynamic response parameter, Cs, which is specified in Item 3.

3.2.1 Method 1

The dynamic loading coefficient, denoted by Cs, is to be calculated using the equation that is provided in the next equation.

$$C_s = \frac{S_a}{\left(\frac{R}{I_e}\right)} \tag{3.2}$$

Here,

Sa is the response acceleration variable that is defined in the Chapter 12.8.2 (ASCE 7-22);

R represents the response modification factor in Table 3.4 (ASCE 7-22); and

Ie is the Importance Factor which can be determined through Table 3.2.

Table 3.4: Table Response Modification Factor Co-Efficient.

Structural System	**R**
RC shear walls (special)	5
RC ductile coupled walls	8
Ordinary RC shear walls	4
Braced frames	8
Special RC shear walls	6
RC ductile coupled walls	8
RC shear walls (ordinary)	5
RC moment frames (special)	5
RC moment frames (intermediate)	3
Ordinary RC moment frames	8

3.2.2 Method 2

The coefficient, Cs, have to be calculated following the equation below.

$$C_s = \frac{S_{DS}}{\left(\frac{R}{I_e}\right)} \tag{3.3}$$

Here,

S_{DS} = Design spectral response acceleration parameter

3.3 THE FUNDAMENTAL TIME PERIOD

The fundamental time limit of the building, T, in the plane that is being considered must be determined by performing an analysis that is sufficiently supported and making use of the structural qualities and deformational features of the components that are resisting deformation. The fundamental period, T, must not be longer than the combination of the variable for the maximum bound on computed period, Cu, which can be found in Table 3.5, and the estimated fundamental period, Ta, which can be calculated by using the equation that is provided in the next sentence.

$$T_a = C_t h_n^x \tag{3.4}$$

Table 3.5: Determination of Parameter Cu.

Spectral Acceleration at 1 s	**Coefficient Cu**
≥ 0.4	1.4
0.3	1.4
0.2	1.5
0.15	1.6
≤ 0.1	1.7

3.4 RESPONSE SPECTRUM ANALYSIS (RSA)

The estimation of the structural response to brief, nondeterministic, time - dependent events can be accomplished through the use of a technique known as response spectrum analysis. Earthquakes and shocks are two examples of these types of phenomena. Because the precise time history of the load cannot be determined, it is difficult to carry out an analysis that is time-dependent. The brief duration of the event precludes the possibility of treating it as an ergodic (or "stationary") process; hence, a random response strategy is not appropriate for this situation. either.

The response spectrum approach utilizes a specialized kind of mode superposition as its fundamental building block. The purpose of providing this input is to establish a limit for the amount that an eigenmode with a specific resonance frequencies and damping may be aroused by an action of this kind.

Types of RSA

a. (SDOF)- Single Degree of Freedom System

b. (MDOF)- Multiple Degree of Freedom System

3.4.1 Analysis of an SDOF System

Take into consideration a mass-spring-damper system that is attached to a base that is moving. The base possesses a predetermined movement denoted by b(t) (Figure 3.7).

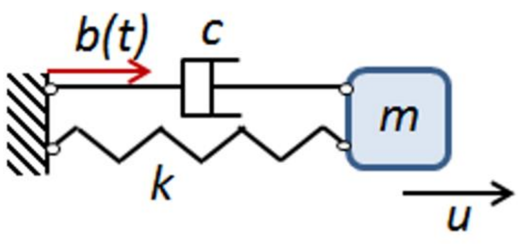

Figure 3.6: SODF System.

If there are no forces acting on the mass from the outside, the motion equation for the mass may be stated as

$$m\ddot{u} + c(\dot{u} - \dot{b}) + k(u - b) = 0 \tag{3.5}$$

Using the conventional system of notation and splitting by the weight,

$$\ddot{u} + 2\zeta\omega_0\dot{u} + \omega_0^2 u = 2\zeta\omega_0\dot{b} + \omega_0^2 b$$

In this case, the natural (angular) frequency that is undamped is

$$\omega_0 = \frac{c}{2\sqrt{km}} \tag{3.6}$$

Where the damping ratio,

$$\zeta = \frac{c}{2\sqrt{km}} \tag{3.7}$$

It is clear that the endorse movement performs the function of a forcing term, while the result requires solely on the two variables ζ and, and not on the specific factors m, c, and k. This may be observed for yourself by looking at the diagram.

It is possible to pick the comparative deformation seen among the mass and the base as the degree of freedom, which is denoted by the equation, $u_r = u - b$.. This is an alternative to choosing the relative displacement as the freedom degree. In reality, this is a frame transformation in which the oscillator is investigated using a coordinate system that is attached to the base. There will always be inertial forces present in any frame that is speeding. It is possible to express the motion equation as

$$\ddot{u}_r + 2\zeta\omega_0\dot{u}_r + \omega_0^2 u_r = -\ddot{b} \tag{3.8}$$

As a result, the acceleration of the support seems to be a weight similar to gravity. This depiction offers two distinct benefits, which are as follows:

a. The internal forces of the system, which include elastic and damping forces, are dependent on the respective displacements and velocities of the system's components. A motion of a rigid body has no effect on these forces.

b. In many cases, the data that has been measured is presented in the form of an accelerogram; hence, the underlying deformations are still not available directly.

This equation may be computed for a reasonably long period of time for a variety of different combinations of ω_0, ζ and *b(t)*. The optimum value that are induced by the acceleration history b are utilized to define the movement, motion, and elastic response spectra b(t).

$$S_d(\omega_0, \zeta, b(t)) = max_t|u_r(t)| \tag{3.9}$$

$$S_v(\omega_0, \zeta, b(t)) = max_t|\dot{u}_r(t)| \tag{3.10}$$

$$S_a(\omega_0, \zeta, b(t)) = max_t|\ddot{u}_r(t)| \tag{3.11}$$

Through the utilization of the relative movement u.

$$S_{d+}(\omega_0, \zeta, b(t)) = max_t u_r(t) \tag{3.12}$$

$$S_{d-}(\omega_0, \zeta, b(t)) = min_t u_r(t) \tag{3.13}$$

It is common practice to approximation the motion and acceleration response spectra using

$$S_v \approx \omega_0 S_d \tag{3.14}$$

$$S_a \approx \omega_0^2 S_d \tag{3.15}$$

As this types tipically called pseudo velocity and pseudo acceleration spectra.

The pseudoacceleration spectrum that is calculated using the relative movement is in fact equivalent to the actual acceleration spectrum when applied to a system that does not include any damping. This may be demonstrated by looking at the equation below

$$\ddot{u}_r + \omega_0^2 u_r = -\ddot{b} \tag{3.16}$$

So,

$$\omega_0^2 u_r = -\left(\ddot{b} + \ddot{u}_r\right) = -\ddot{u} \tag{3.17}$$

Therefore, the point in time at which the highest magnitude of the relative motion coincides with the point in time at which the highest upper bound of the relative acceleration must take place. The scale factor that differentiates the two is denoted by ω_0^2. This correlation will remain roughly valid even for systems that have a low level of dampening. It is typical to make the assumption that such spectra for the actual acceleration as well as the pseudoacceleration are identical. This is due to the fact that the majority of propulsion parts have a low damping (generally 2% to 5%).

The Q factor is an additional frequent method that is used to describe the absorption in this situation. The equation that describes the connection to that same damping ratio is as follows:

$$Q = \frac{1}{2\zeta} \tag{3.18}$$

3.4.2 Multiple DOF System

Let's say a numerical equation of a structure is segmented using FEM in such a way which the motion equations in matrix form are as follows:

$$\mathrm{M}\ddot{\mathrm{u}} + \mathrm{C}\dot{\mathrm{u}} + \mathrm{K}\mathrm{u} = \mathrm{f}(t) \tag{3.19}$$

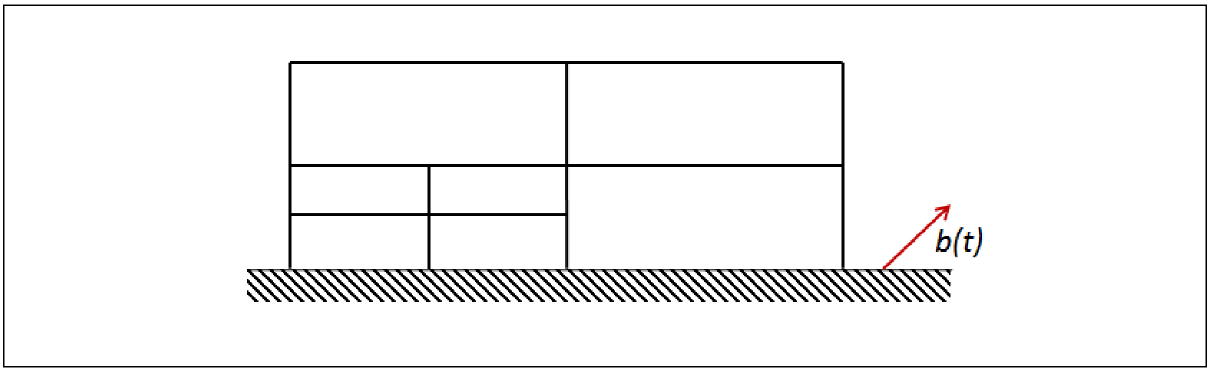

Figure 3.7: MDOF System.

The base motion of the building is determined by the fact that it is connected at a variety of locations to a single "ground" (t). This vector is the same size as u , which represents the entire number of DOFs; however, it only includes three distinct characteristics: : $b_x(t)$, $b_y(t)$, and $b_z(t)$. Now, the entity is denoted by the notation $\mathrm{u}_r = \mathrm{u} - \mathrm{b}$. If there is no load from the outside, the motion equation is.

$$\mathrm{M}(\ddot{\mathrm{u}}_r + \ddot{\mathrm{b}}) + \mathrm{C}\dot{\mathrm{u}}_r + \mathrm{K}\mathrm{u}_r = 0 \tag{3.20}$$

or

$$\mathrm{M}\ddot{\mathrm{u}}_r + \mathrm{C}\dot{\mathrm{u}}_r + \mathrm{K}\mathrm{u}_r = -\,\mathrm{M}\ddot{\mathrm{b}} \tag{3.21}$$

Here, viscous forces in the system is used, as a result, $\mathrm{Kb} = \mathrm{C}\dot{b} = 0$

$$\text{By solving } (\mathrm{K} - \omega^2\mathrm{M})\phi = 0 \tag{3.22}$$

$$\Phi = [\phi_1\phi_2 \quad \cdots \quad \phi_N] \tag{3.23}$$

In accordance with the conventional procedures for modal overlap, the decoupled modal solutions are as follows:

$$\ddot{q}_j + 2\zeta_j\omega_j\dot{q}_j + \omega_j^2 q_j = -\phi_j^T\mathrm{M}\ddot{\mathrm{b}} \tag{3.24}$$

It has been taken for granted that perhaps the weight matrix normalizing of the eigenmodes will be applied, as well as the damping matrix will be able to be diagonalized mostly by eigenmodes. The normalizing of the mass matrix is not required, however doing so will make some formulas easier to understand.

Here, qj denotes the fundamental coefficient for mode j; hence, one may express the relative displacement as a linear function of eigenmodes, with the weighting determined mostly by modal coordinate values:

$$\mathrm{u}_r = \Phi\mathrm{q} \tag{3.25}$$

The support motion

$$\mathrm{b}(t) = b_x(t)1_x + b_y(t)1_y + b_z(t)1_z \tag{3.26}$$

The number "1" is assigned to all degrees of freedom (DOFs) that pertain to X-translation, whereas the value "0" is assigned to all other DOFs. Therefore, the equation of motion for modes of motion is.

$$\ddot{q}_j + 2\zeta_j\omega_j\dot{q}_j + \omega_j^2 q_j = -\phi_j^T\mathrm{M}\big(\ddot{b}_x(t)1_x + \ddot{b}_y(t)1_y + \ddot{b}_z(t)1_z\big) = -\Gamma_{xj}\ddot{b}_x(t) - \Gamma_{yj}\ddot{b}_y(t) - \Gamma_{zj}\ddot{b}_z(t) \tag{3.27}$$

Here the multipliers r_{kj}, And,

$$\Gamma_{kj} = \phi_j^T \mathrm{M} 1_k \tag{3.28}$$

Therefore, when loaded by a fundamental motion in the direction k defined by a response spectrum, the peak amplitude of mode j equals

$$\hat{q}_{kj} = S_d\big(\omega_j, \zeta_j, b_k(t)\big)\Gamma_{kj} \tag{3.29}$$

In another words the pseudo acceleration spectrum

$$\hat{q}_{kj} = \frac{S_a\big(\omega_j,\zeta_j,b_k(t)\big)\Gamma_{kj}}{\omega_j^2} \tag{3.30}$$

In a nutshell, the peak amplitude of a particular eigenmode is calculated by multiplying the response spectrum value at the associated natural frequency (which is unaffected by the structure) by the participation factor.

3.5 CALCULATION PROCEDURE OF RSA IN THIS THESIS

3.5.1 Parameters

3.5.1.1 g

It is the gravitational Acceleration

3.5.1.2 Site class

It is required that the soil at the site be categorized in line with Table 3.6.

Site Class F: A soil type that contains soils that are susceptible to probable failure during earthquake loads, such as cohesionless soils, fast and incredibly sensitive clays, and compressible weakly cemented soils, is called a seismically vulnerable soil profile.

Site Class A: Its measured between the hard rock types of soil. These measurements must be performed in order to support the category. These measures may be carried out either on the premises or away from the premises. In regions where it is known that the characteristics of hard rock are continuous down to a depth of one hundred feet or more (30 m)

Site Class B: This sort of terrain will include conditions that are medium hard to soft rock sites.

Site Class E: When a site does not meet the requirements for Site Class F and there is a total thickness of soft clay that is greater than 10 feet (3 meters), and when a soft clay layer is defined as having su that is less than 500 psf (su that is less than 25 kPa), then the site is considered to be in Site Class G.

Table 3.6: Site Class Values.

Site Class	**Vs**
Hard rock	greater than 5,000
Medium hard rock	In between 3,000 to 5,000
Soft rock	In between 2,100 to 3,000
Medium dense sand or stiff clay	In between 700 to 1,000
Loose sand or medium stiff clay	In between 500 to 700
Very loose sand or soft clay	Less than 500

3.5.1.3 R

According to Table 3.4 of Design Coefficients and Factors for Seismic Force-Resisting Systems, the response modification coefficient.

3.5.1.4 Risk category

The risk coefficient was calculated based on Table 3.1.

3.5.1.5 Importance Factor (Ie)

Importance factor is calculated according to Table 3.2

3.5.1.6 Seismic design category

Earthquake Design Class E must be allocated to any building in a region with a Risk Category I, II, or III if the calculated spectral response acceleration constant at the 1-s interval, S1, is more than or equal to 0.75. Structures belonging to Risk Category IV that are located in areas in which the estimated spectral response acceleration factor at 1-s period, S1, is more than or equal to 0.75 must be classified as belonging to Seismic Design Category F. The seismic design category that should be applied to every other structure is determined by the risk level associated with it as well as the designed spectral response acceleration parameters, Ss and S_1, that are calculated. The seismic design category according to Table 3.7 is given below.

Table 3.7: Table for Determining Ss.

Site Class	$S_s \leq 0.25$	$S_s = 0.5$	$S_s = 0.75$	$S_s = 1.0$	$S_s \geq 1.25$
A	0.8	0.8	0.8	0.8	0.8
B	1	1	1	1	1
C	1.2	1.2	1.1	1	1
D	1.6	1.4	1.2	1.1	1
E	2.5	1.7	1.2	0.9	0.9

3.5.1.7 Evaluation of Response Spectrum

The following requirements should be attained by the design RSA

a. At period, T, equal to 0 seconds, 0.01 seconds, 0.02 seconds, 0.03 seconds, 0.05 seconds, 0.075 seconds, 0.1 seconds, 0.15 seconds, 0.2 seconds, 0.25 seconds, 0.3 seconds, 0.4 seconds, 0.5 seconds, 0.75 seconds, 1.0 seconds, 1.5 seconds, 2.0 seconds, 3.0 seconds, 4.0 seconds, 5.0 seconds, 7.5 seconds, and 10 seconds, the 5%-damped design RS parameter, Sa.

b. If the reaction time, T, is shorter than 10 seconds but is not equal to any of the discrete data of period, T, provided in Item 1 above, then Sa is selected by linear interpolation between both the values of Sa, of Item 1 above.

c. If T ≤ T_L, Sa is calculated as even the rate of Sa just at period of 10 s of Item 1 above multiplied by 10/T; and where T > T_L, Sa is calculated as that of the value of Sa at the period of 10 s multiplied by 10 T_L/T_2.

d. The value of the model spectral response acceleration variable, Sa, is to be determined in accordance with the equation that is shown in the next paragraph.

$$S_a = S_{DS}\left(0.4 + 0.6\frac{T}{T_0}\right) \tag{3.31}$$

e. The model spectral response acceleration factor, S_a, is to be taken as equal to S_{DS} for all periods that begin after T_0 and end before T_s. This applies to all periods that begin after T_0 and end before T_s.

f. The model spectral response acceleration factor, S_a, should be regarded as indicated in the following equation for periods that are higher than T_s and smaller than or equivalent to T_L.

$$S_a = \frac{S_{D1}}{T} \tag{3.32}$$

g. The Periods higher than T_L, S_a shall be taken as given in the following equation.

$$S_a = \frac{S_{D1}T_L}{T^2} \tag{3.33}$$

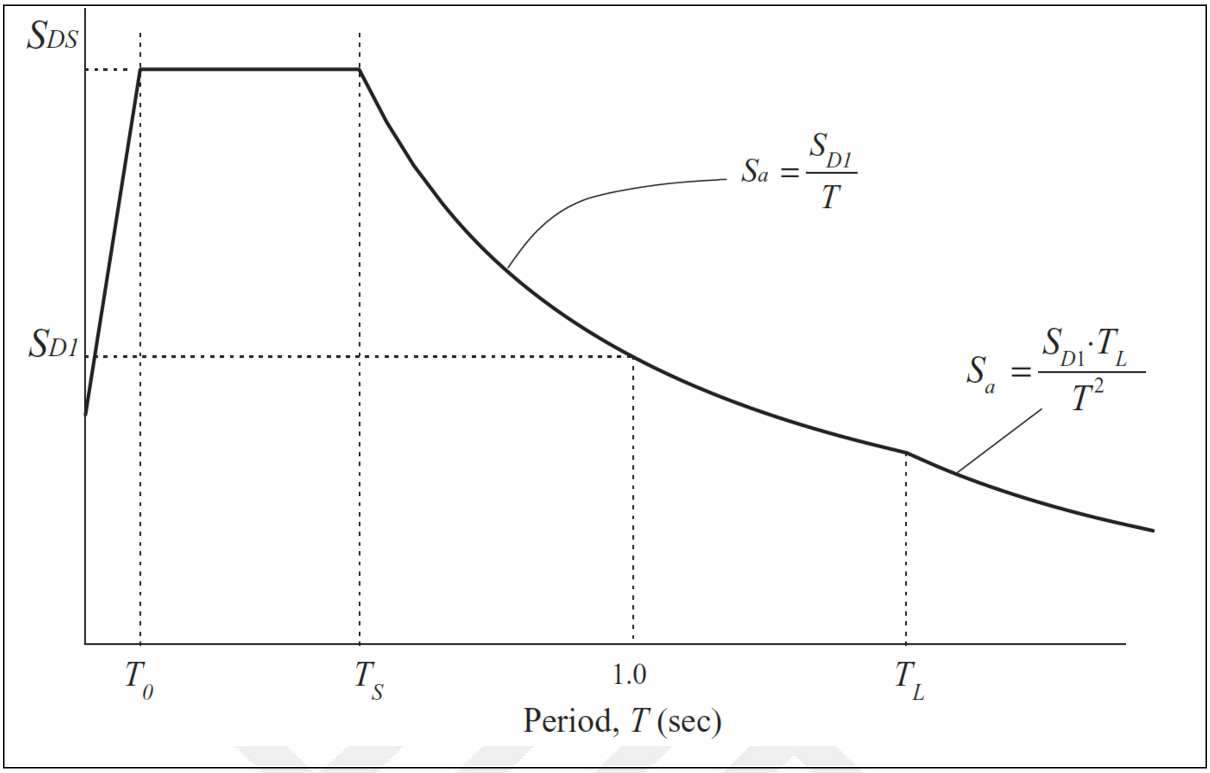

Figure 3.8: Design Spectral Acceleration.

3.5.1.8 Maximum value of T

$$T_{max} = C_u T_a \tag{3.34}$$

Cu is taken from Table 3.5

The following is an approximation of the basic time periods that buildings have existed:

$$T_a = C_t h_n^x \tag{3. 35}$$

Here,

T_a is the estimate time period

h_n represents the height of the top to the reference floor.

C_t as well as the value x obtained from Table 3.8

Table 3.8: Coefficient for Ct and x.

Structure	C_t	x
Steel MRF system	0.0724	0.8
Concrete MRF system	0.0466	0.9
Every single one of the other structural systems	0.0488	0.75

3.6 STRUCTURAL MODEL

ETABS is utilized in order to carry out the analysis for the plan of the high-rise construction. In the course of the research, a rectangular floor design for a high-rise building of fifty stories was taken into consideration. The third-dimensional finite element analysis was applied to a total of three different models, including RCC Moment Resisting Frame (MRF) model [Figure 3.10], Core shear wall model [Figure 3.11], Shear wall at the corner end model [Figure 3.12]. The models are denoted as Case-1, Case-2 and Case-3 respectively.

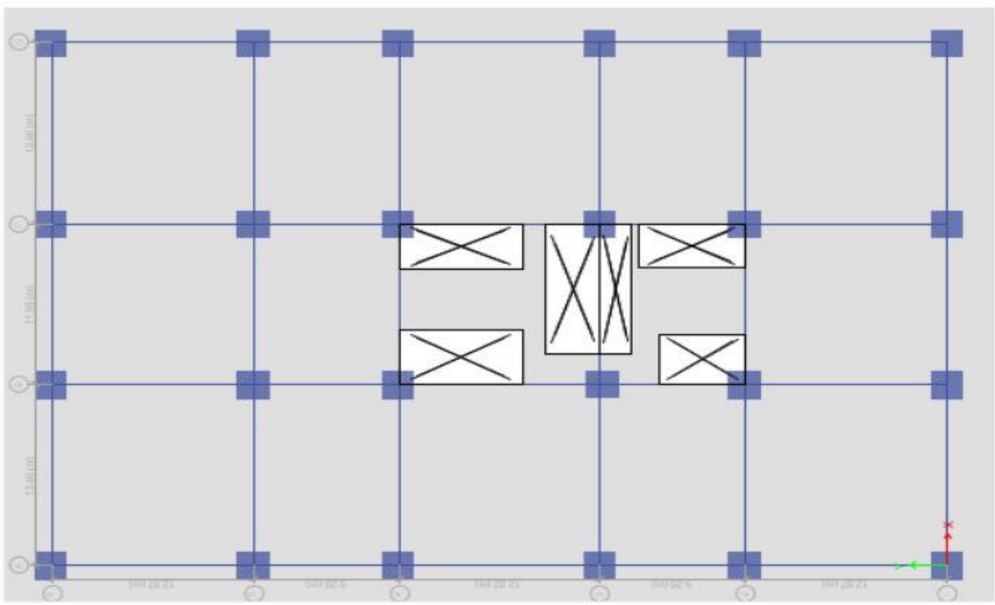

Figure 3.9: Moment Resisting Frame Model (Case-1).

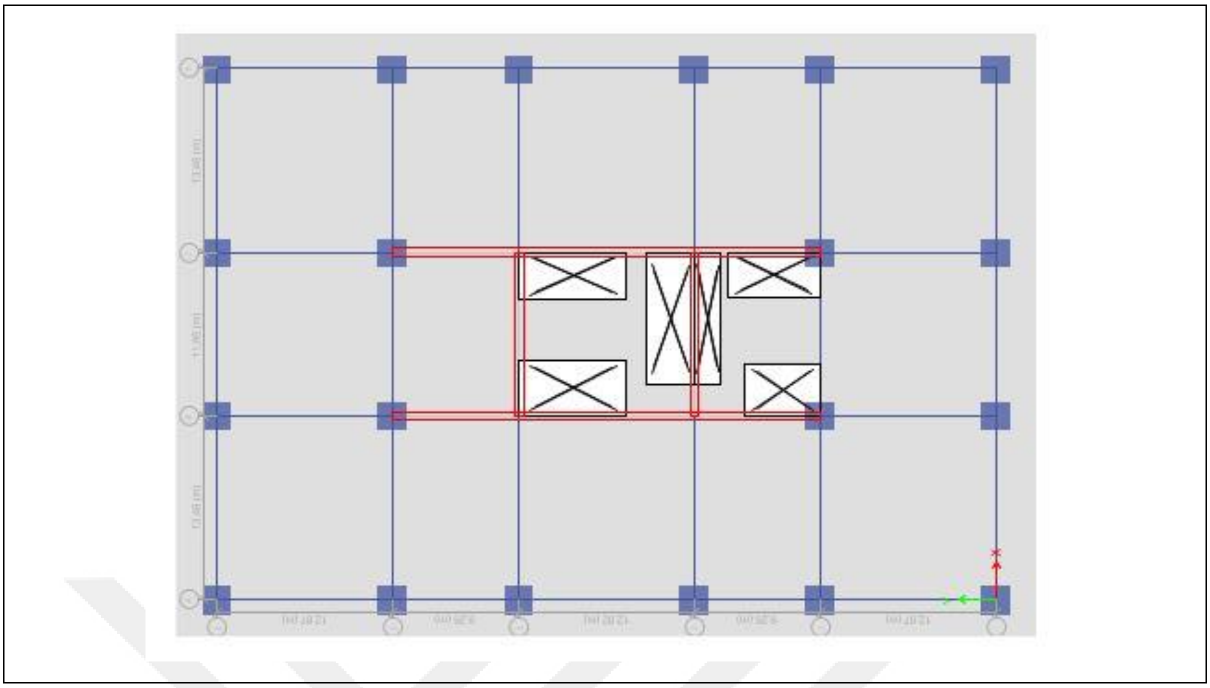

Figure 3.10: Core Shear Wall Model (Case-2).

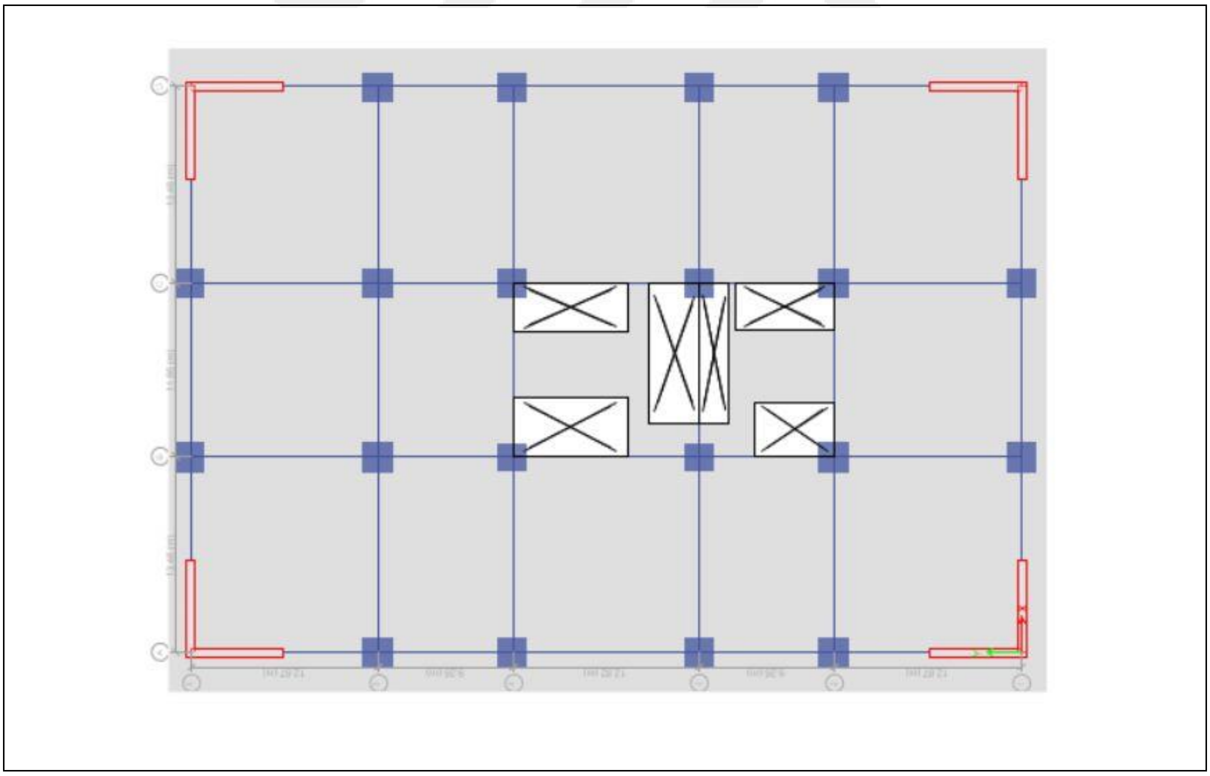

Figure 3.11: Shear Wall at Corner End Model (Case-3).

Figures 3.13 and 3.14 show the three-dimensional elevations of Case-1 and Case-2, while Figure 3.13 shows the three-dimensional elevation of Case-3.

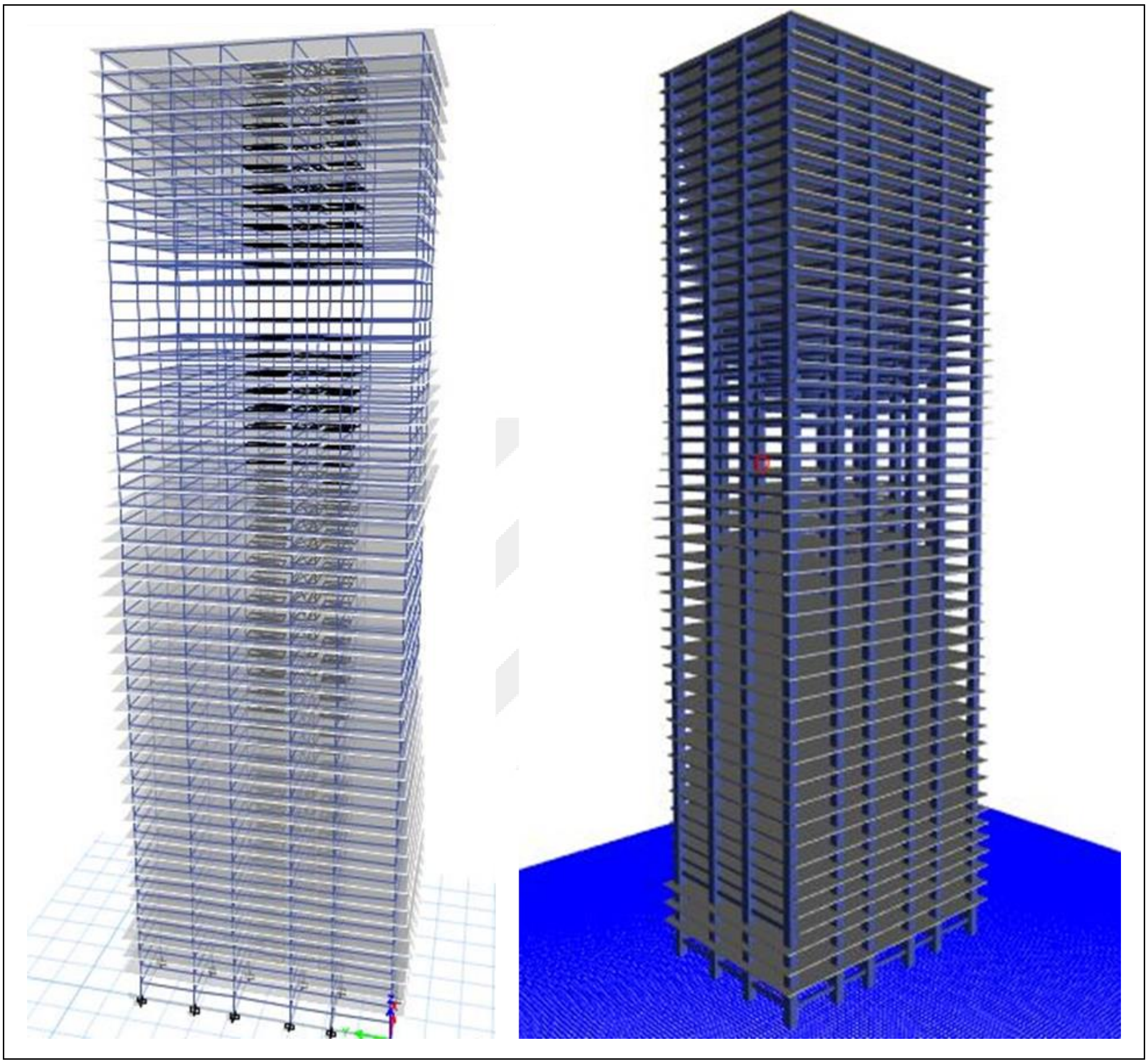

Figure 3.12: 3-D view of Case-1.

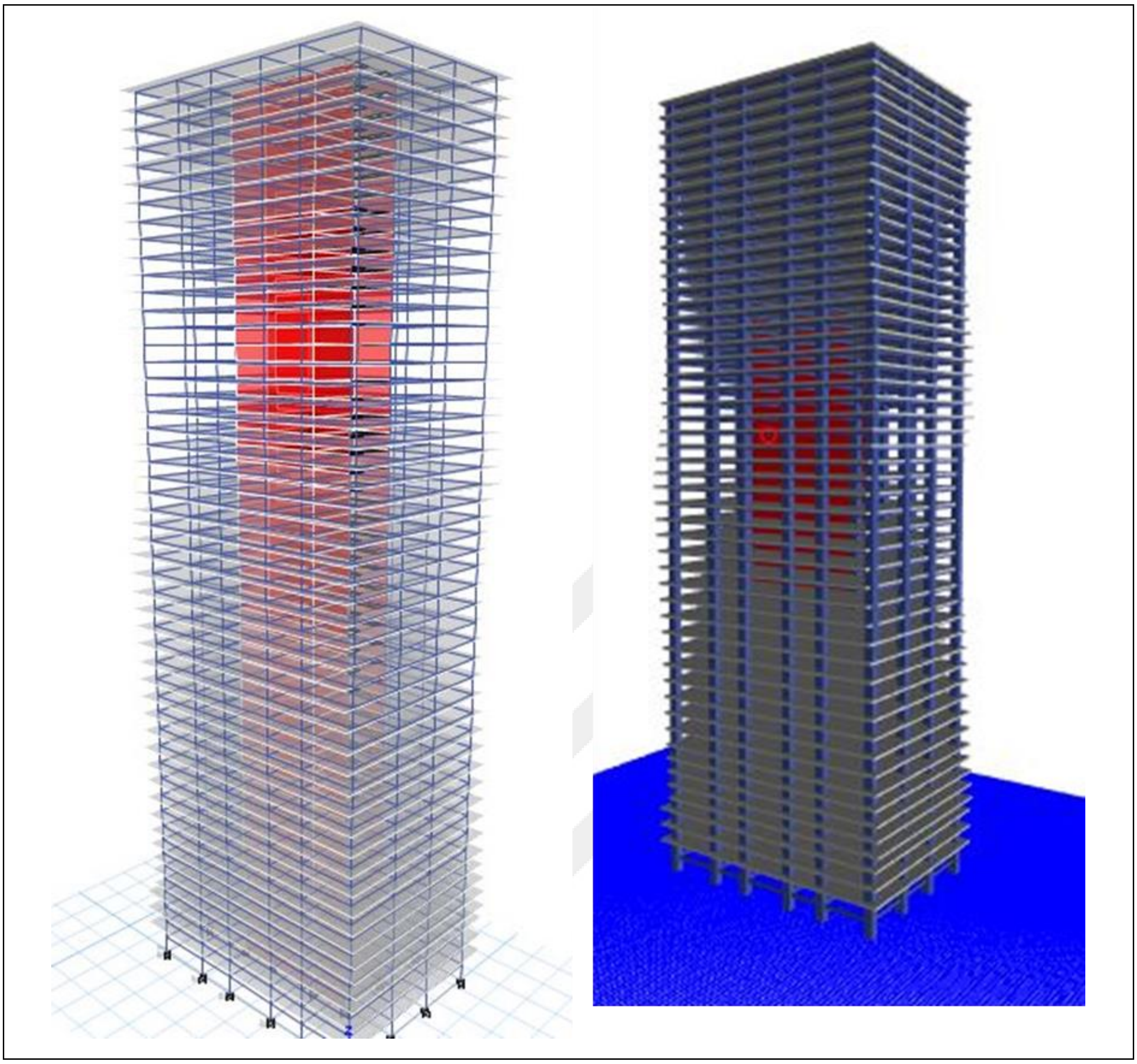

Figure 3.13: 3-D view of Case-2 Model.

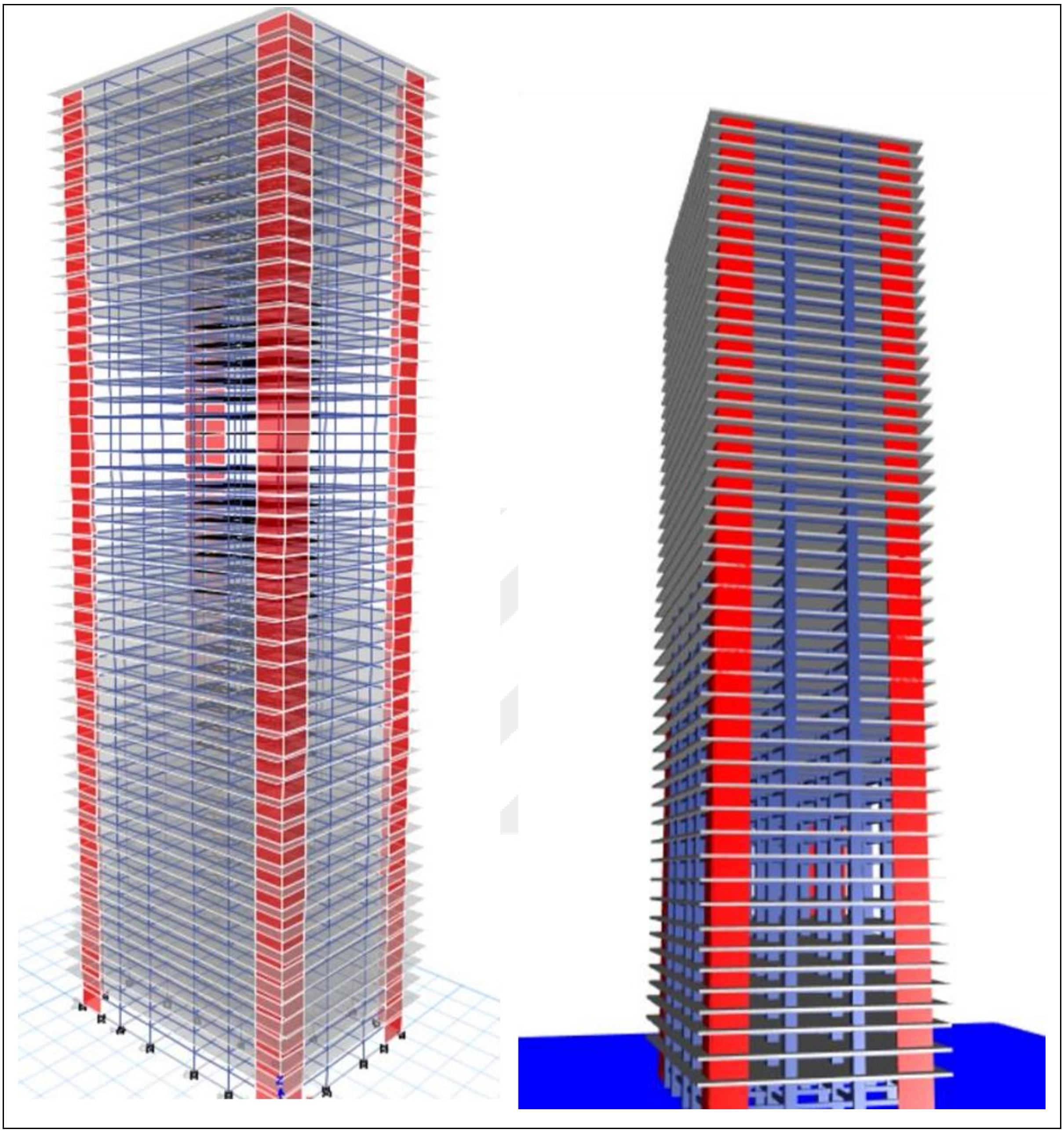

Figure 3.14: 3-D View of Case-3.

3.6.1 Material Properties

In this analysis, the grade of concrete known as C55 was used for all of the analytical models' columns and shear walls, whereas the grade known as C45 was used for the beams, slabs, and outrigger systems. The concrete and steel reinforcing requirements utilized in the construction are shown in Table 3.9. The thickness of the slab in each model was set at 300 millimeters, and the size of the column was set at 2,100 millimeters by 2,100 millimeters. Furthermore, the breadth direction of the beam was estimated to be 350 millimeters, while the depth direction was estimated to be 550 millimeters.

Table 3.9: Material Properties.

Material	E (MPa)	ν	Density (kg/m^3)	ε_u	Compressive strength (MPa)	F_y (MPa)	F_u (MPa)
C45	31529	0.18	2400	0.002	45	-	-
C55	34857	0.18	2400	0.002	55	-	-
Rebar	210000	0.2	7850	0.3		250	420

3.6.2 Loading Data

In this research, the models are studied using linear dynamic analysis in compliance with ASCE 7-22 regulations. (ASCE-7-22, 2022). The service dead load was determined to be 3.5 kN per square meter for each model in this inquiry, and the live load was determined to be 4.0 kN per square meter.

3.6.3 Analysis Procedure

The first step in the Response Spectrum approach is to calculate the highest response value in each mode of a structure using a spectrum curve. Once this value is found, the approach uses model superposition to integrate the answers. In general, a building's reaction is a mix of many modes, and in this case, the Square Root Sum of the Square approach was used. Once the modal load scenario was defined, ASCE [53] code spectral acceleration data was generated. (Figure 3.16). The data was then transformed into ETABS using the textual format. The data for all seismic zones were created on the basis of the soft soil condition Sc. Following a linear static analysis, a response spectrum load scenario was created. The original scale factor was Ig/R, where 'g' is gravity's acceleration, 'I' is the importance factor, and 'R' is the response modification coefficient for the various frame categories mentioned in the preceding sections. Based on the data, a modal analysis was done on all of the models. Because the algorithm allows for a minimum of 90% of the static base shear, the scaling factor was changed once more after the study. The mode number was also changed to meet with the rule's requirement of a minimum modal mass participation ratio of 90%. Following each adjustment, the mathematical models were subjected to a new study in line with the ASCE code.

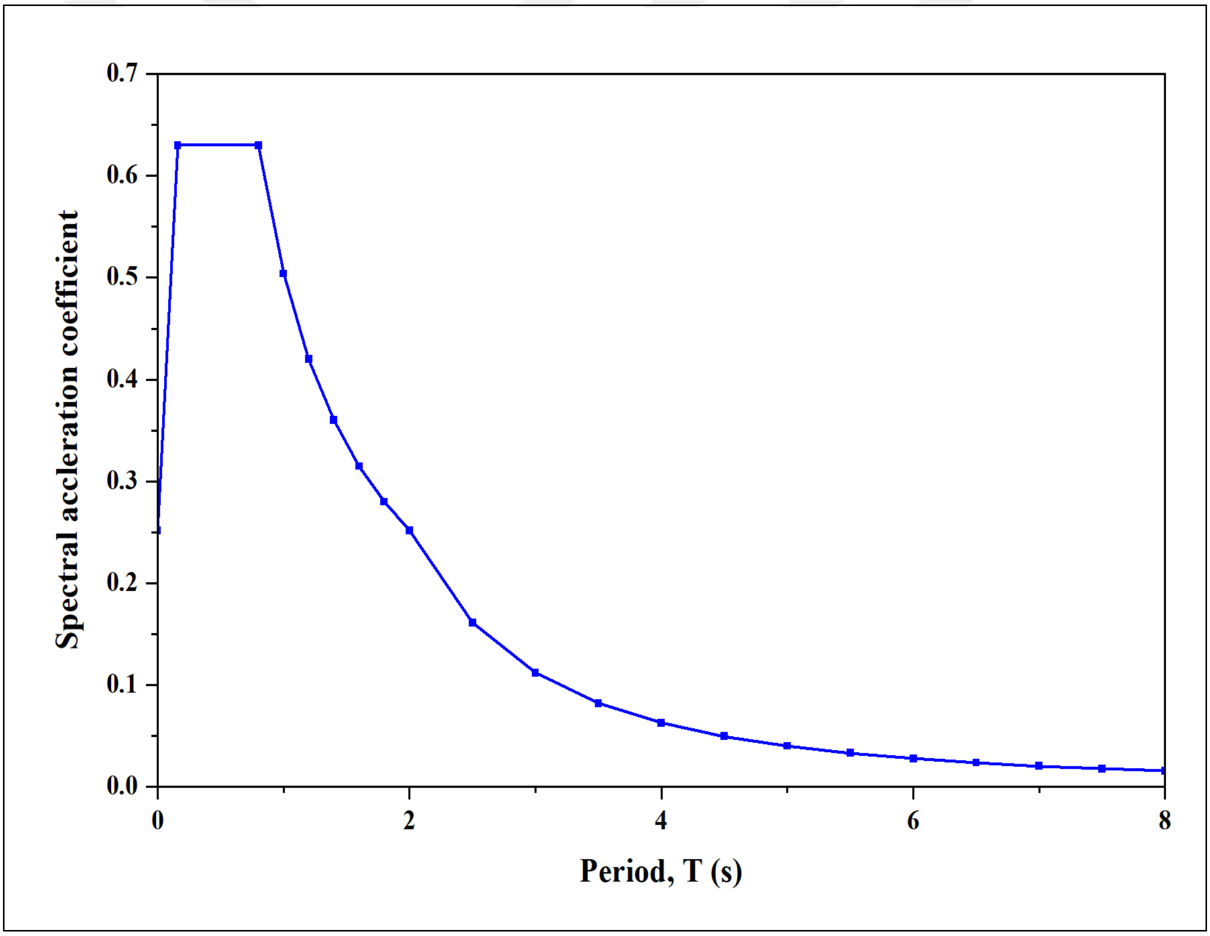

Figure 3.15: Applied Spectral Acceleration Data.

4. RESULTS AND DISCUSSION

4.1 STORY DISPLACEMENTS

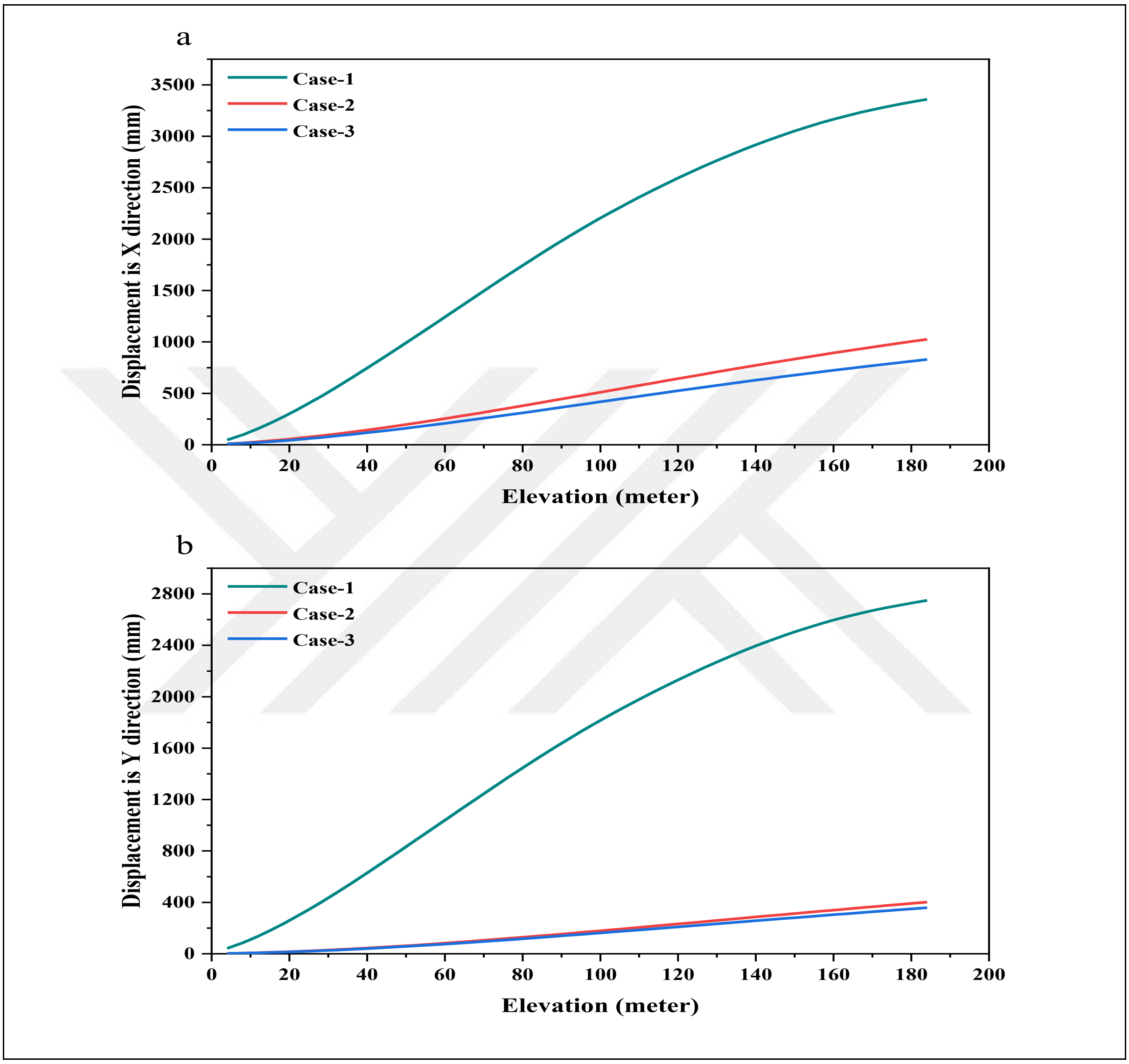

Figure 4.1: Total Story Displacement for X and Y Directions.

Figure 4.1 depicts the outcomes of the story displacement analysis performed on each and every one of the produced models. The model that consisted of shear walls at the corners performed better as the dynamic analysis was carried out; the displacement was the lowest for this Case-3 in both the global-X and global-Y direction. For this model, the greatest displacement in the global X direction was 829.556 mm, and the minimum displacement was 7.035 mm. However, the maximum displacement in the global Y direction was only

358.404 mm, which is a significant decrease from the global X direction. On the other hand, the Case-2 model, which included a shear wall at the core, likewise demonstrated a significant reduction in displacement in both directions. For this particular model, the greatest displacement in the global-X direction was 1025.9 millimeters, while the minimum displacement was 9.14 millimeters. The maximum displacement in the global-Y direction was 402 millimeters. However, case-1, which only included MRF, demonstrated a displacement that was on average 304% and 667% larger in the global-X and global-Y directions, respectively, as compared to case-3, which featured the model with the best overall performance. For this particular model, the greatest displacement in the global-X direction was 3359.5 mm, while the minimum displacement that could occur was 47.21 mm. The maximum displacement that could occur in the global-Y direction was 2750 mm. The model that consisted just of a moment resisting frame represented the maximum displacement because there was no stiffer structure to resist the seismic forces. Ahamad and Pratap [54] also studied the robust effect that shear walls have on structures. As a consequence of this, the combined effect of shear walls in case-3, both at the core and in all of the corners, exhibited the best performance possible against seismic forces.

4.2 MAXIMUM ALLOWABLE STORY DRIFT

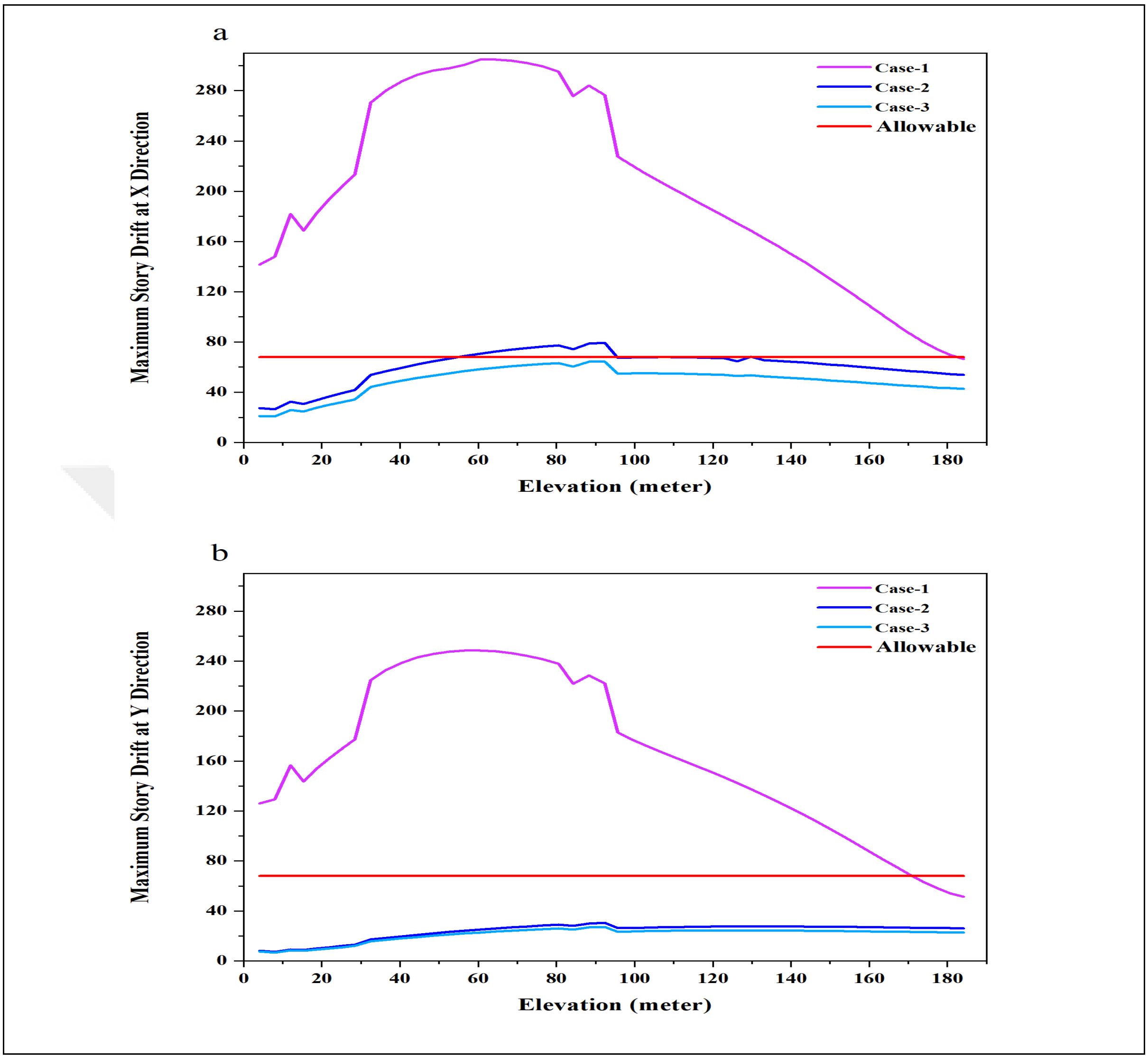

Figure 4.2: Total Story Drift Results for X and Y Directions.

The greatest amount of story drift that may be tolerated is shown in Figure 4.2 for each of the models that were produced. It is easy to observe from the image that the shear wall was a significant factor in controlling the drift in the global-X direction and the global-Y direction correspondingly. The Case-1 model, which just featured a moment resistant frame, was unable of reducing the drift values to levels that were acceptable within the permitted limit. The permissible drift was determined using the guideline of ASCE 7-22, which is also included in Table 3.1 for your convenience. The value of acceptable drift that was achieved was 68. The story's drift values for the Case-1 model ranged from a high of 304.8 to a low of 2483, with the smallest values being 66.39 and 51.28 in the global-X and Y directions, respectively. The Case-1 model had the greatest and lowest values for the story drift when compared to the other models. The graphical depiction shows that the majority of the stories for the Case-1 model did not pass the test according to the acceptable level.

On the other hand, the overall drift values for the Case-3 model ranged from a minimum of 20.83 to a high of 64.49 in the X direction and 27.32 in the Y direction correspondingly. The least value was 6.78 and the maximum value was 64.49. In addition, the greatest value of the story drift for the Case-2 model was 79.23 and 30.50, while the minimum value was 26.43 and 6.31 in the X and Y directions respectively. This was the case for both X and Y directions. Both the Case-2 and the Case-3 models, which both consisted of a shear wall, were successful in keeping the drift within the permissible limit.

4.3 STORY DRIFT RATIO

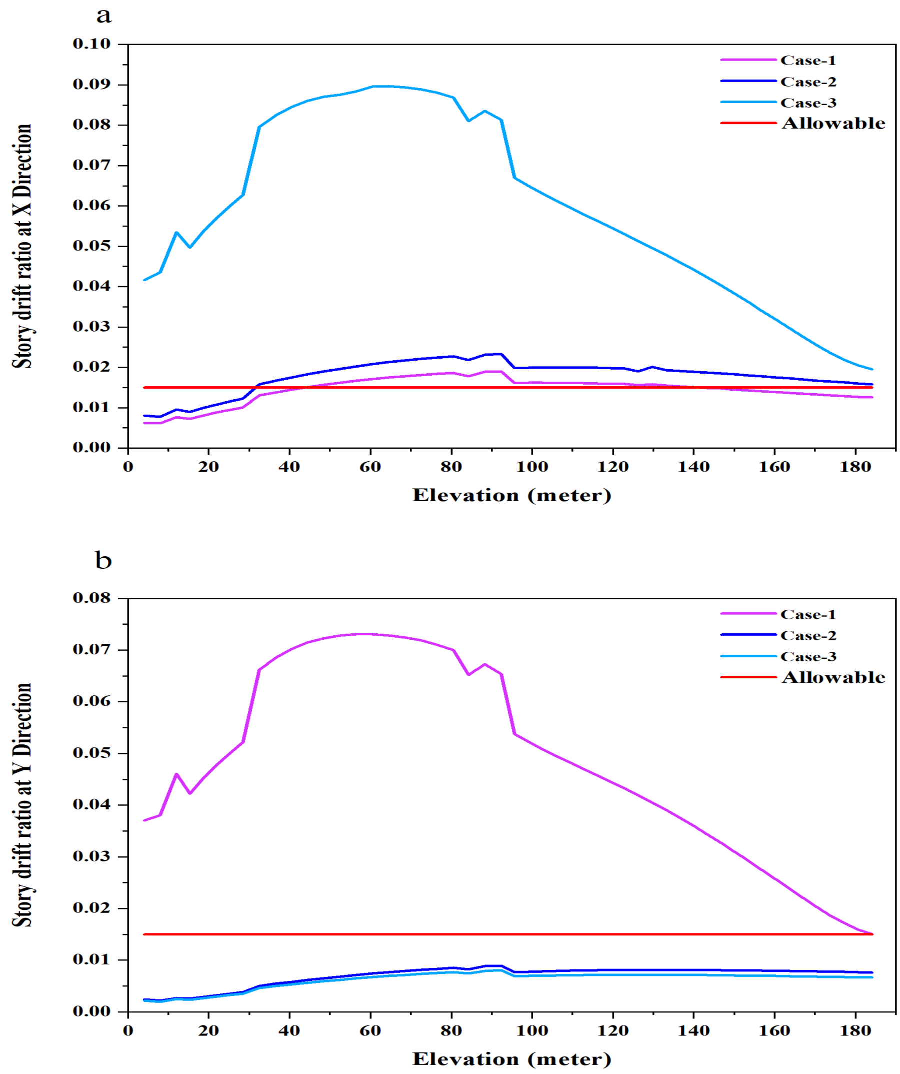

Figure 4.3: Maximum and Allowable Drift Ratio Comparison for Both Directions.

The findings of the allowable story drift proportions are shown in figure 4.3. These values are displayed for each model that has been developed. It is abundantly evident from looking at the image that the shear wall was an essential component in the process of controlling the drift ratios in both the global-X and global-Y directions. The Case-1 model, which just featured a moment resistant frame, was unable to manage the drift ratio values to levels that were acceptable within the permissible limit. The permissible drift was determined using the guideline of ASCE 7-22, which is also included in Table 3.1 for your convenience. The value of the permissible drift ratio that was found was 0.015. For the Case-1 model, the maximum value for the tale drift ratio was found to be 0.018 and 0.073, while the smallest value was determined to be 0.0061 and 0.015 in both the X and the Y directions, respectively. The graphical depiction shows that the majority of the stories for the Case-1 model did not pass the test according to the acceptable level.

Besides, the maximum story drift ratio for Case-2 model was 0.023 and 0.0089 at both X and Y direction respectively. On the other hand, the minimum story drift ratio for Case-2 model was 0.0077 and 0.0021 at both X and Y direction respectively. Additionally, for Case-3 model, the maximum value of the story drift ratio was 0.089 and 0.0080 while the minimum value was 0.0195 and 0.0019 at both X and Y direction respectively. Both Case-2 and Case-3 model consisting shear wall were able to keep the drift ratio value under the allowable limit.

4.4 STORY STIFFNESS

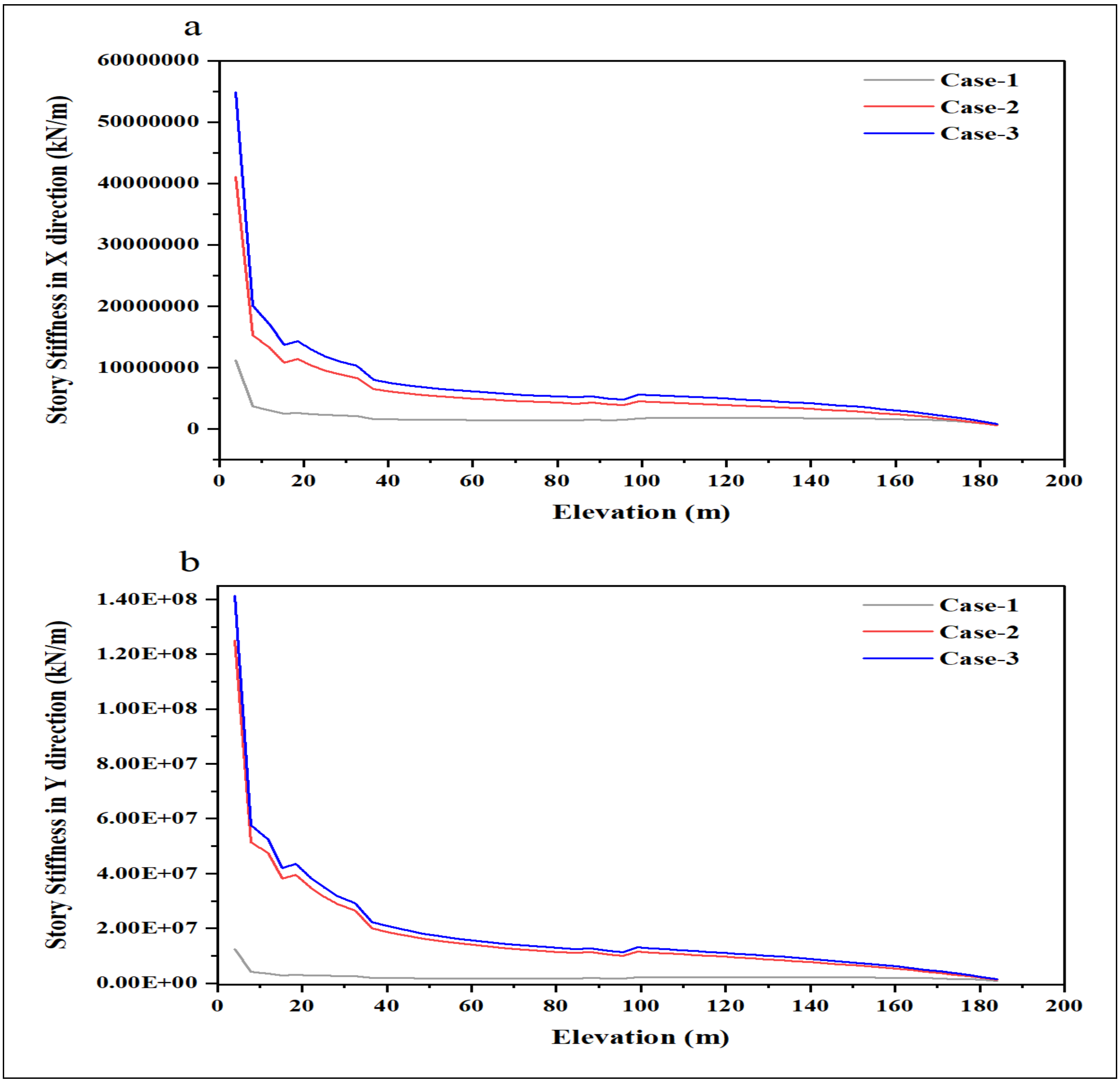

Figure 4.4: Obtained Stiffness Values for The Models.

The values of the overall story stiffness are displayed in figure 4.4 for each of the created models. When subjected to a dynamic study, the model that included shear walls at the corners performed significantly better, and in Case 3, the stiffness was greatest in both the global-X and global-Y directions. For this model, the greatest displacement in the global X direction was 54822696 kN/m, while the minimum displacement was determined to be 364823 kN/m. On the other hand, the maximum displacement in the worldwide Y direction was 141269214 kN/m, which is a substantial increase from the global X direction. The Case-

2 model, which consisted of a shear wall at the core, exhibited significant enhancements in stiffness in both directions as well. This model had a maximum story stiffness of 41075835 kN/m, while the lowest story stiffness for the global-X direction was 288688 kN/m and the maximum displacement for the global-Y direction was 124977340 kN/m. The highest story stiffness for the global-Y direction was 41075835 kN/m. However, case-1, which included solely MRF, demonstrated the least amount of stiffness in the tale. This particular model had a maximum overall narrative stiffness of 11191458 kN/m. On the other hand, the global-X direction had the lowest story stiffness, which was 324404 kN/m. The global-Y direction had the highest maximum displacement, which was 12411618 kN/m.

.

4.5 STIFFNESS IRREGULARITY

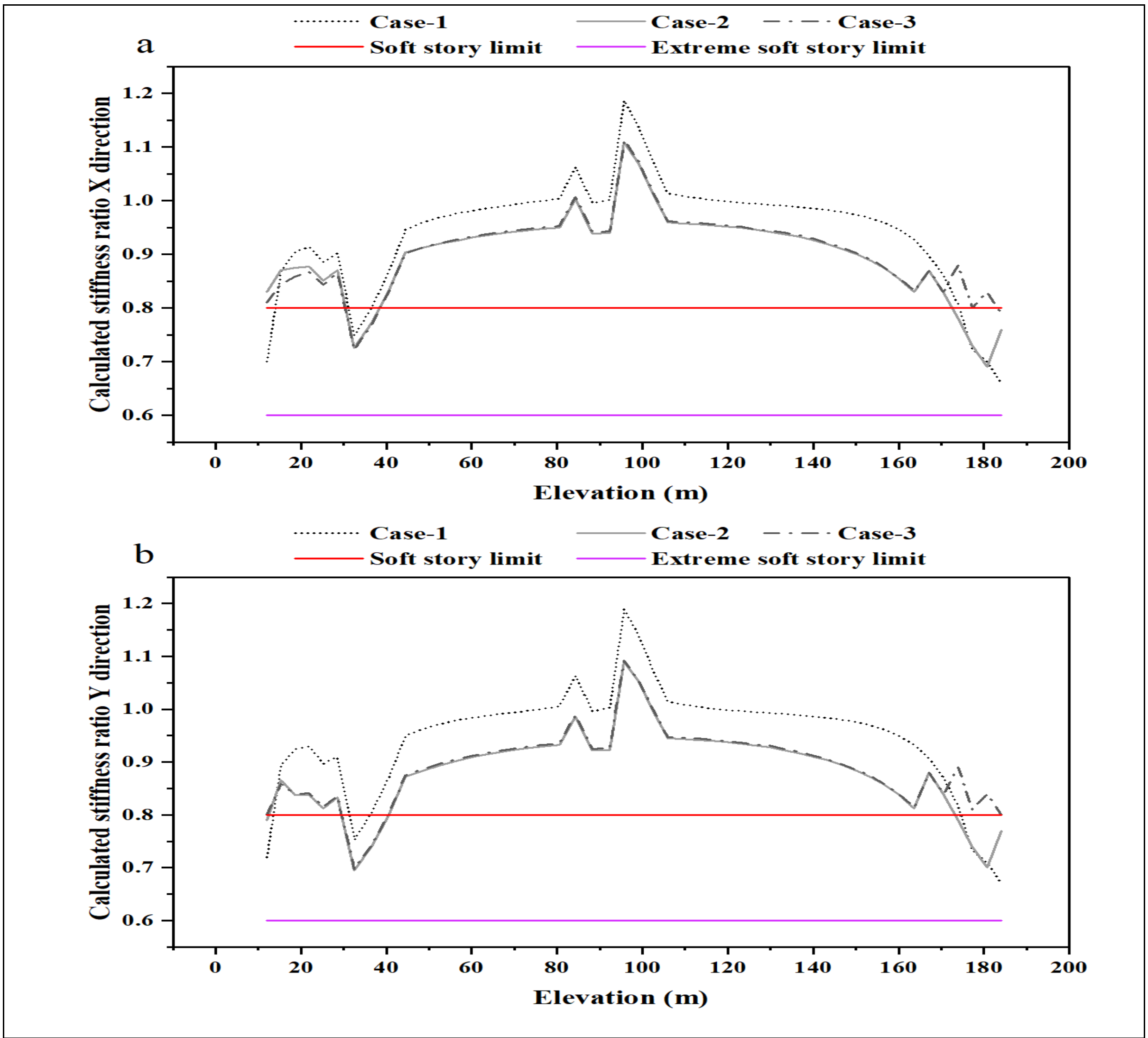

Figure 4.5: Calculated and Allowable Story Stiffness Ratios for Both Directions.

Figure 4.5 is a demonstration of the allowable story stiffness ratios for each of the models that were developed. It is abundantly evident from looking at the image that the shear wall played a significant part in the process of controlling the stiffness ratios in both the global-X direction and the global-Y direction. Each of the models, including the Case-1 model, which consists just of a moment-resistant frame, was also able to regulate the majority of the stiffness ratio values within the permissible limit. This was the case even though the model only had one component. The maximum permissible stiffness was determined using the guideline found in ASCE 7-22, which may also be found in chapter 3 of this book. The value of the permissible drift ratio that was obtained was 0.8 for the soft narrative and 0.6 for the extremely soft story. The Case-1 model had the highest value of 1.186 and 1.187 for the narrative stiffness ratio, while the Case-1 model had the lowest value of 0.66 and 0.67 for the tale stiffness ratio in the X and Y directions respectively. According to the depiction of the graphical representation, the majority of the tests for the Case-1 model were successful and fell within the acceptable range.

On the other hand, the narrative stiffness ratio for the Case-2 model had a maximum value of 1.1088 and 1.1089 and a minimum value of 0.698 and 0.694 in the X and Y directions, respectively. In addition, the maximum story stiffness ratio for the Case-3 model was 1.11, and it was 1.09 in the X direction and the Y direction separately. On the other hand, the minimal ratio of minimum story stiffness for the Case-3 model was 0.72 in the X direction and 0.69 in the Y direction correspondingly. Both the Case-2 and the Case-3 models, which both consisted of a shear wall, were successful in maintaining a stiffness ratio value that was below the permissible limit.

4.6 BASE SHEAR

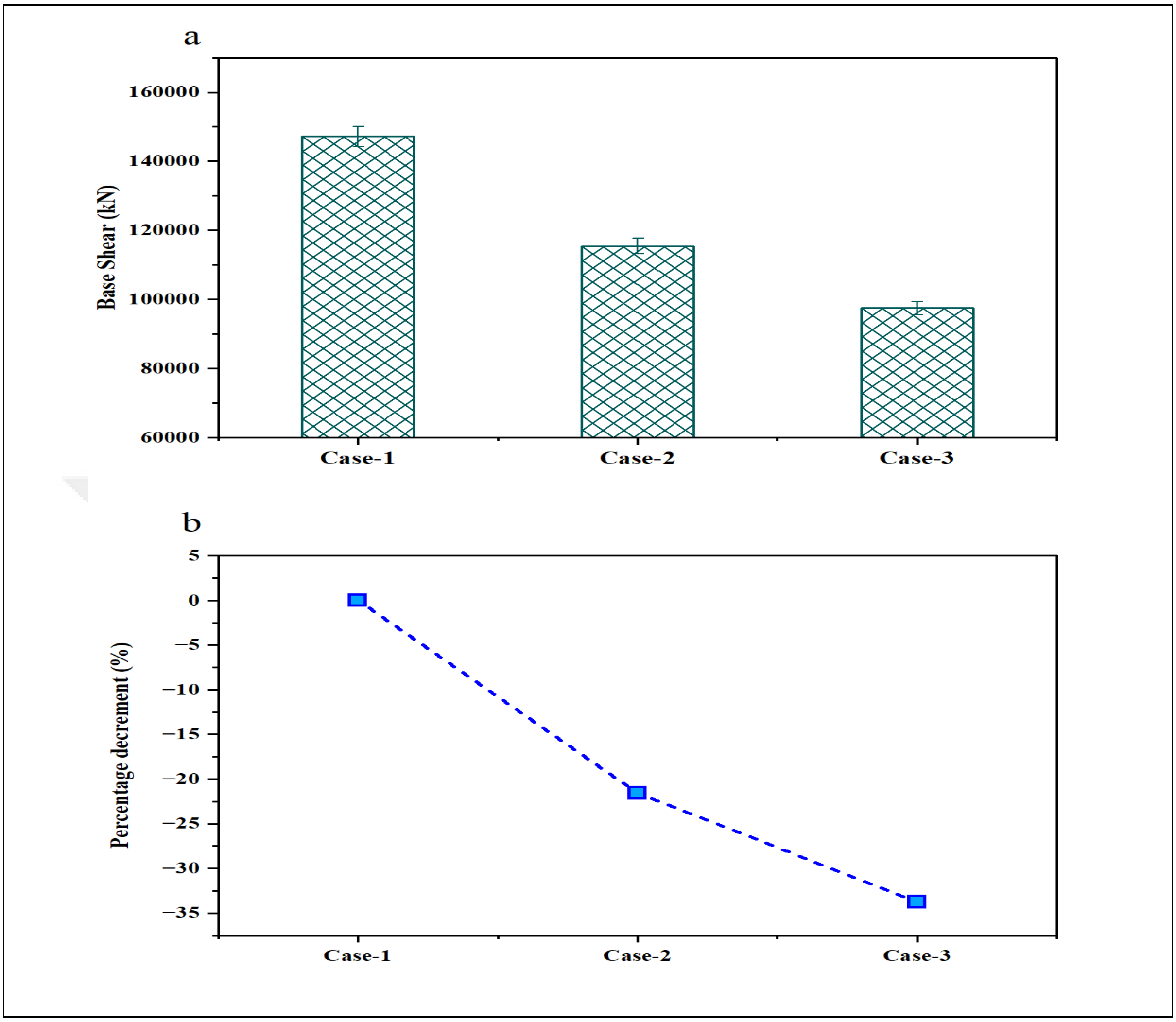

Figure 4.6: Obtained Base Shear and The Comparison of Base Shear Change in %.

The shear values at the base are displayed in figure 4.6 for all of the models that have been developed. The results of the dynamic analysis show that the model with shear walls at the corners performed far better, and for Case 3, the base shear was the lowest it could be in both the global-X and global-Y directions. This conclusion may be drawn from the findings of the study. This particular model has a maximum base shear value of 97483 kN. On the other hand, the Case-2 model, which displayed base shear of 115433 kN despite being subjected to the seismic stress, consisted of a shear wall at the core. This base shear value was 21% lower than the value calculated using the Case-1 model, which only includes the moment resisting frame. Case-1, which solely featured MRF, had base shear that was almost 33 percent higher than the top-performing model in Case-3. This model has a shear value of

147166 kN as its starting point. Because it lacked a more rigid framework to mitigate earthquake stresses, the model that just had a moment-resisting frame displayed the largest base shear under the ground acceleration.

4.7 FUNDAMENTAL TIME PERIOD

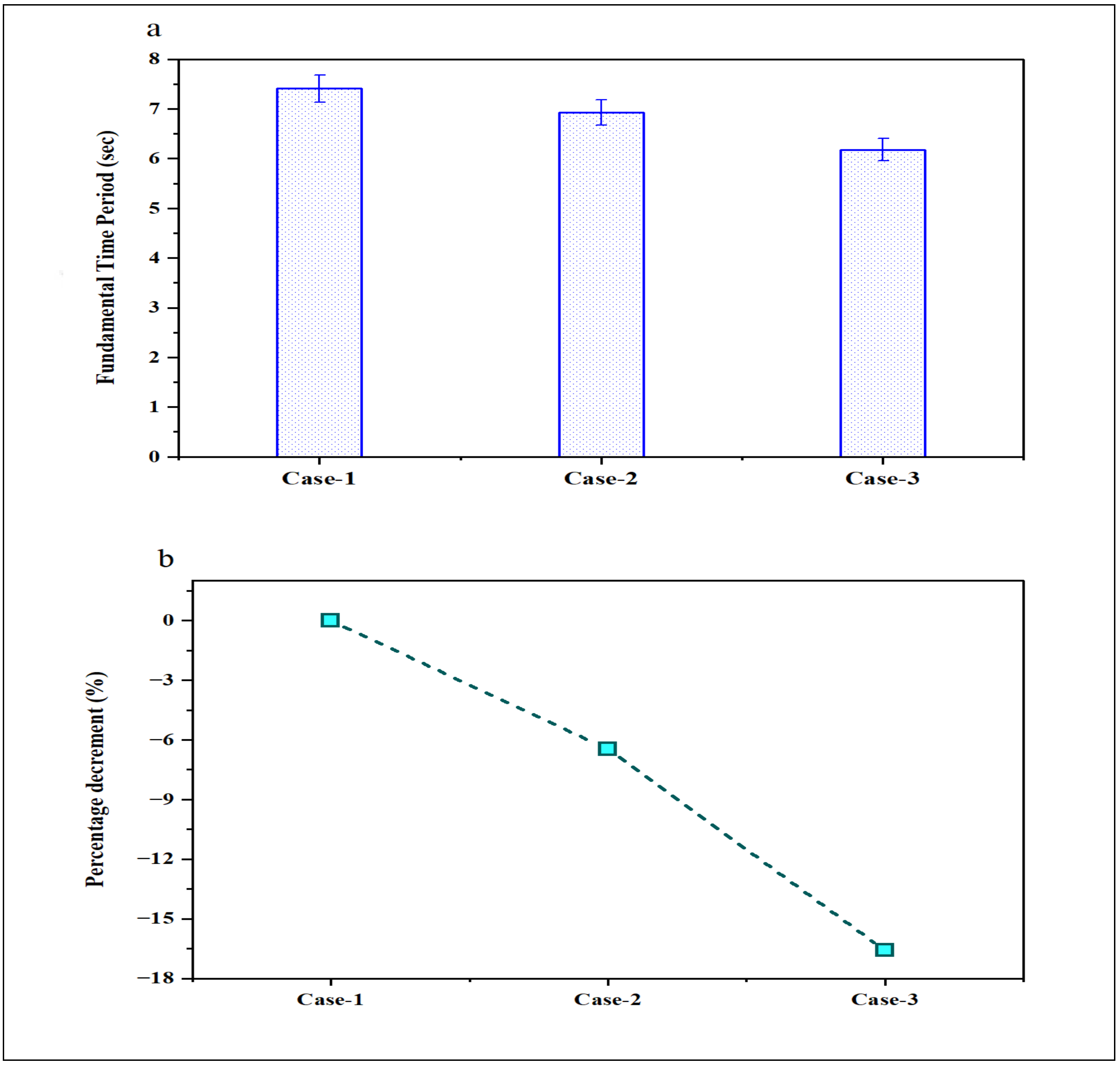

Figure 4.7: Obtained Time Period and The Comparison of Time Period Change in %.

Figure 4.7 is an illustration of the outcomes of the fundamental time period for the models that were produced. Based on the findings of the dynamic study, it is clear that the model consisting of shear walls at the corners performed significantly better than the others; the Case-3 variant had the fundamental time period that was the shortest. For this particular model, the greatest fundamental time period was 6.18 seconds. In contrast, the Case-2 model, which consists of a shear wall at the core, likewise exhibited a fundamental time period of 6.93 seconds when subjected to the seismic force. This basic time period value was 7% lower than the number that was calculated using the Case-1 model, which only includes the moment resisting frame. Case-1, which just made use of MRF, demonstrated a basic time period that was 16% faster than the top-performing model in Case-3. For this particular model, the basic time period value was 7.41 seconds. After performing the response spectrum analysis, each and every fundamental time period was successfully achieved, and a model mass participation ratio of more than 90% was ensured.

4.8 STORY FORCE

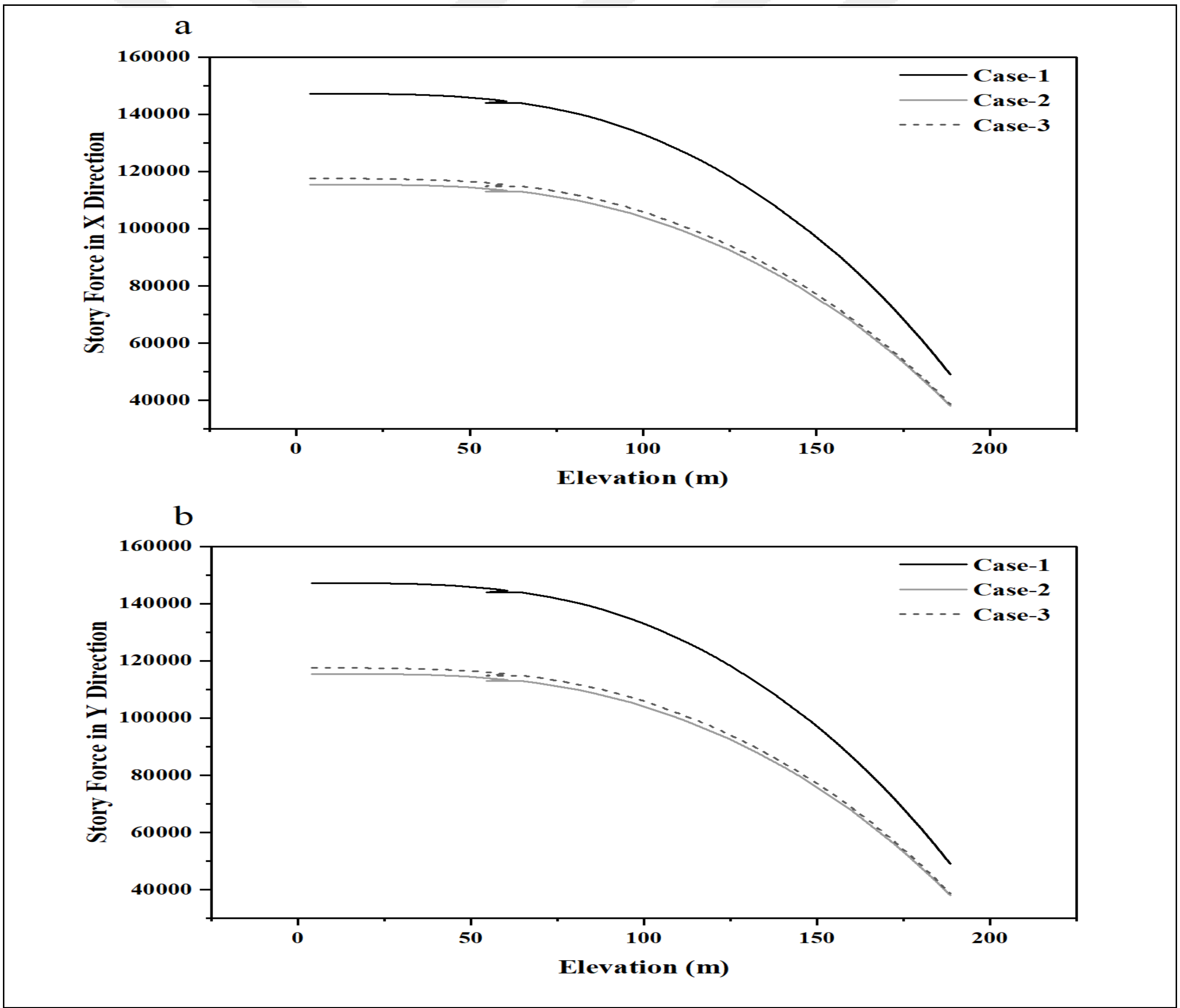

Figure 4.8: Obtained Story Force vs Story Height Values at Both Directions.

Figure 4.8 displays the story force values for each generated model. From the figure it can clearly be seen that shear wall played an important role to control the story force both in the global-Y as well as the global-X direction respectively. Each of the models, including Case-1 model which consisting only moment resisting frame was also able to control most of the story force levels. For Case-1 model, the highest story force was found 147166 kN whereas the minimum value was 48932 kN at both the Y and X direction respectively. The graphical representation illustrates that most of the story force for all the developed model and the change in the story force value with the change of elevations.

On the other hand, the minimum story force vale for Case-2 model was 37977 kN while the largest value was found 115433 kN at both X and Y direction respectively. Additionally, for Case-3 model, the highest and lowest story force was found 97482 kN and 38581 kN at both the X and the Y direction respectively. Both Case-2 and Case-3 models consisting of shear wall were able to keep the story force value significantly less than the Case-1 model.

4.9 TORSIONAL IRREGULARITY

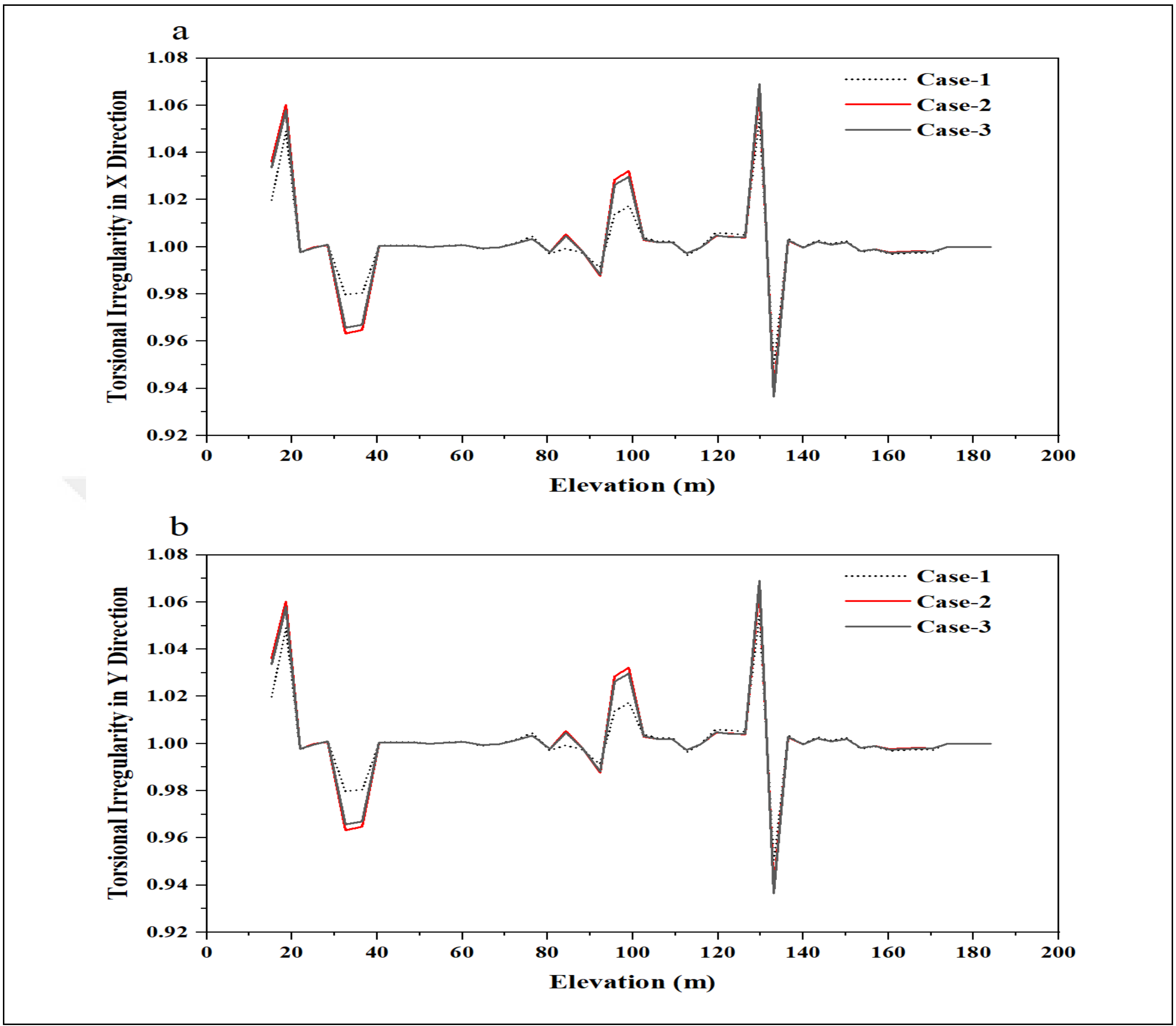

Figure 4.9: Comparison of The Torsional Irregularity Values at Both Direction.

Figure 4.9 depicts the story mass-weight ratio findings for all developed models. From the figure it can clearly be seen that shear wall was crucial in controlling its entire story mass-weight ratio in the global-X as well as the global-Y direction. Every models including Case-1 model which consisting only moment resisting frame was also able to control the story torsional irregularity under the allowable limit. The allowable story mass-weight ratio for torsional irregularity was calculated from the guideline of ASCE 7-22, which is also presented in chapter 3. The obtained allowable story mass-weight ratio value was 1.2 for torsional irregularity and for extreme torsional irregularity, it was 1.4. For Case-1 model, the maximum story mass-weight ratio was 1.053 and 1.057 whereas the minimum story stiffness ratio was 0.948 and 0.949 at both the X and Y direction respectively. The graphical representation illustrates that all of the story for Case-1 model passed according to the allowable limit.

Conversely, the maximum mass-weight ratio for Case-2 model was 1.068 and 1.066 while the minimum value was 0.937 and 0.939 at both X and Y direction respectively. Additionally, the maximum value of the mass-weight ratio for Case-3 model was 1.069 and 1.066 at both X and Y direction respectively. On the other hand, the minimum mass-weight ratio for Case-3 model was 0.964 and 0.938 at both X and Y direction respectively. Both Case-2 and Case-3 model consisting of shear wall were able to keep the mass-weight ratio value under the allowable limit.

4.10 MAXIMUM OVERTURNING MOMENT

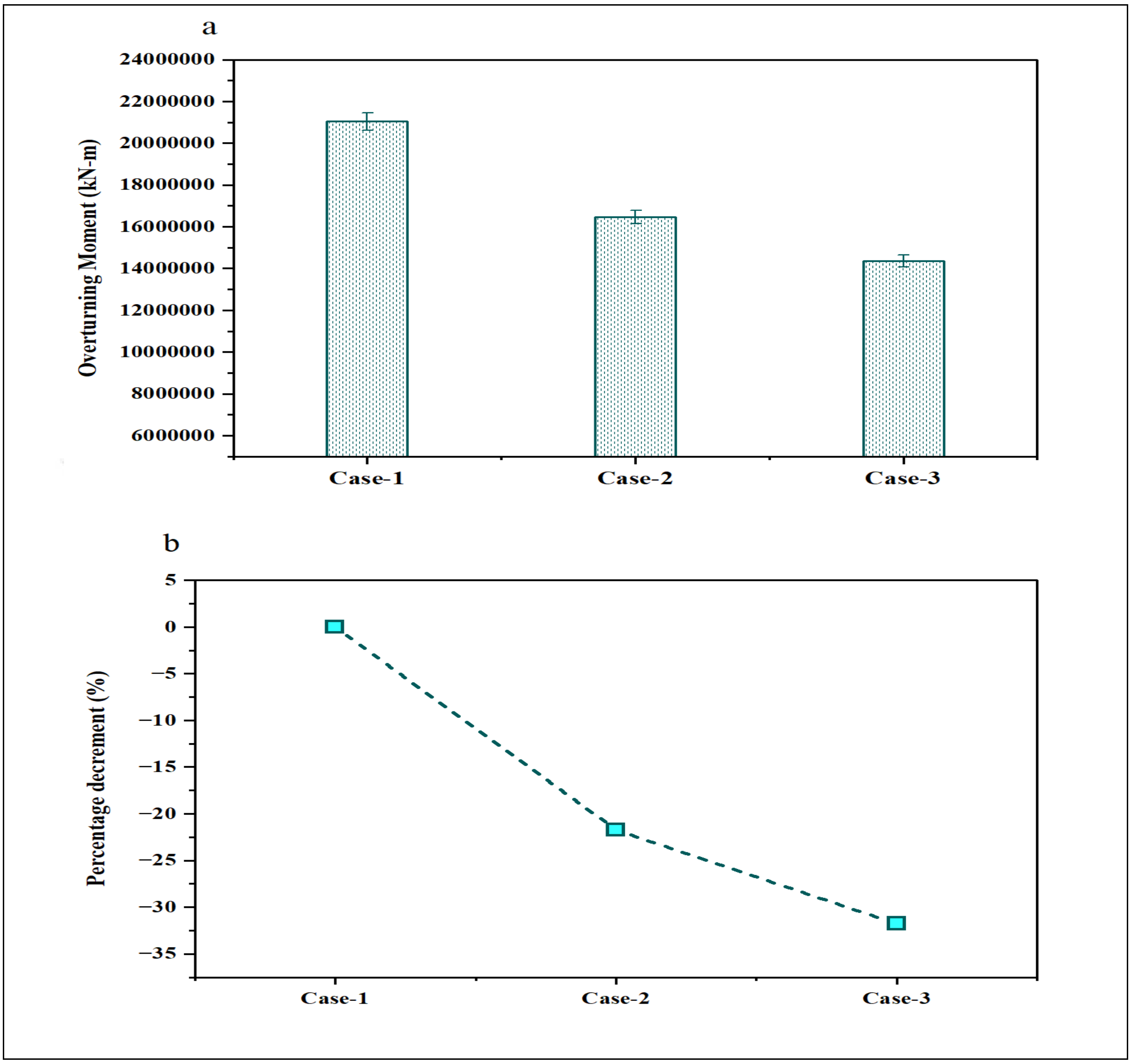

Figure 4.10: Obtained Story Overturning Moment and The Comparison of The Change in %.

Figure 4.10 illustrates the results of maximum overturning moment for the developed models. From the dynamic analysis, it can be found that the model having shear wall at the corners performed better; the maximum overturning moment was the lowest for this Case-3. The maximum overturning moment for this model was 14354459 kN-m. On the other hand, Case-2 model consisting of shear wall at the core also depicted the maximum overturning moment which was 16465904 kN-m under the seismic load. This maximum overturning moment value was 21.8% less than the Case-1 model which only consists of moment resisting frame. The Case-1, which solely contained MRF, displayed a maximum average overturning moment that was 31.7% higher than the case-3's top-performing model. For this model, the highest overturning moment was 21040643 kN-m. All the maximum overturning moment was obtained after the response spectrum analysis, with ensuring more that 90% model mass participation ratio.

5. CONCLUSION

Buildings constructed in accordance with the approach experienced base shears that were many times more than their design values whenever exposed to response-spectrum-compatible artificial ground motions. Therefore, it was possible to compare the shear-wall positions for moment-resisting frame scenarios in which substantial amounts of inelastic deformations are anticipated. The dynamic analysis yields the following conclusions:

a. It was discovered that by reinforcing the high-rise building with a structural model, the displacement and story drift that occur as a result of ground motion may be contained within acceptable parameters.

b. When compared to the MRF model, the use of shear walls not only in the core but also at the corners has a substantial influence on control structure displacement as well as horizontal irregularities and overturning moment. The use of shear walls at the four corners of the structure is the most appropriate method for controlling the stiffness irregularity of the high-rise structural system. This is because shear walls are designed to be used at corners. In terms of the amount of story displacement, the model that consisted of shear walls at the corners (Case-3), displayed 300% less story displacement than the MRF model did. (Case-1). Additionally, in comparison to the Case-1 model, the Case-2 model, which consisted of a core shear wall, displayed 21% less base shear, and the Case-3 model, which depicted 34% less base shear.

c. Compared to the MRF theory, the use of an infill walls in the sidewalls and the heart significantly affects the system stability motion, lateral anomalies, and overturning moment. Structural systems so at three walls of the structure are the most practical method for controlling the strength inconsistency of the rising framed structure. In terms of horizontal irregularities, the MRF model failed to keep the values under the allowable limit in most of the cases, where shear-wall depicted significant improvement in every cases.

d. Torsional Irregularity was not observed both in global-X and global-Y direction due to the regular rectangular shape of the structures.

e. Because the model with shear wall at corners as well as core shear wall performed the best, it can be further analyzed for all of seismic zones and soil conditions whether to see if the model was still able to keep seismic displacement and drift within allowable limits.

REFERENCES

[1] E. Baran, H. C. Mertol, and B. Gunes, "Damage in reinforced-concrete buildings during the 2011 Van, Turkey, earthquakes," *Journal of Performance of Constructed Facilities,* vol. 28, no. 3, pp. 466-479, 2014.

[2] H. B. Ozmen, M. Inel, and B. T. Cayci, "Engineering implications of the RC building damages after 2011 Van Earthquakes," *Earthq. Struct,* vol. 5, no. 3, pp. 297-319, 2013.

[3] M. Fintel, "Shearwalls-an answer for seismic resistance?," *Concrete International,* vol. 13, no. 7, 1991.

[4] S. Satpute and D. Kulkarni, "Comparative study of reinforced concrete shear wall analysis in multistoreyed building with openings by nonlinear methods," *Int. J. Struct. & Civil Engg,* vol. 2, no. 3, 2013.

[5] Ö. Avşar and O. Tunaboyu, "Influence of structural walls on the seismic performance of RC buildings during the May 19, 2011 Simav Earthquake in Turkey," *Journal of Performance of Constructed Facilities,* vol. 28, no. 4, p. 04014016, 2014.

[6] N. Haghi, S. Epackachi, and M. T. Kazemi, "Macro modeling of steel-concrete composite shear walls," in *Structures*, 2020, vol. 23, pp. 383-406: Elsevier.

[7] R. Rahnavard, A. Hassanipour, M. Suleiman, and A. J. J. o. B. E. Mokhtari, "Evaluation on eccentrically braced frame with single and double shear panels," vol. 10, pp. 13-25, 2017.

[8] M. Naghavi, R. Rahnavard, R. J. Thomas, and M. J. J. o. B. E. Malekinejad, "Numerical evaluation of the hysteretic behavior of concentrically braced frames and buckling restrained brace frame systems," vol. 22, pp. 415-428, 2019.

[9] R. Rahnavard, M. Naghavi, M. Aboudi, and M. J. C. S. i. C. M. Suleiman, "Investigating modeling approaches of buckling-restrained braces under cyclic loads," vol. 8, pp. 476-488, 2018.

[10] R. Rahnavard, A. Hassanipour, and A. J. J. o. C. S. R. Mounesi, "Numerical study on important parameters of composite steel-concrete shear walls," vol. 121, pp. 441-456, 2016.

[11] N. Haghi, S. Epackachi, and M. T. Kazemi, "Cyclic performance of composite shear walls with boundary elements," in *Structures*, 2020, vol. 27, pp. 102-117: Elsevier.

[12] B. Shafei, F. Zareian, and D. G. J. E. S. Lignos, "A simplified method for collapse capacity assessment of moment-resisting frame and shear wall structural systems," vol. 33, no. 4, pp. 1107-1116, 2011.

[13] S. Radkia, R. Rahnavard, H. Tuwair, F. A. Gandomkar, and R. Napolitano, "Investigating the effects of seismic isolators on steel asymmetric structures considering soil-structure interaction," in *Structures*, 2020, vol. 27, pp. 1029-1040: Elsevier.

[14] S. Etedali, K. Hasankhoie, and M. R. J. J. o. B. E. Sohrabi, "Seismic responses and energy dissipation of pure-friction and resilient-friction base-isolated structures: A parametric study," vol. 29, p. 101194, 2020.

[15] A. Lanzi and J. E. J. J. o. S. E. Luco, "Elastic velocity damping model for inelastic structures," vol. 144, no. 6, p. 04018065, 2018.

[16] C.-S. Tsai, Y.-M. Wang, and H.-C. J. I. J. o. O. I. Su, "SOIL-STRUCTURE INTERACTION, DAMPING AND HIGHER MODE EFFECTS ON THE RESPONSE OF A MID-STORY-ISOLATED STRUCTURE FOUNDED ON MULTIPLE SOIL LAYERS," vol. 1, no. 3, 2019.

[17] C. Adam, L. F. Ibarra, and H. Krawinkler, "Evaluation of P-delta effects in non-deteriorating MDOF structures from equivalent SDOF systems," 2004.

[18] E. Miranda and S. D. J. J. o. S. E. Akkar, "Dynamic instability of simple structural systems," vol. 129, no. 12, pp. 1722-1726, 2003.

[19] E. B. J. J. o. S. E. Williamson, "Evaluation of damage and P-Δ effects for systems under earthquake excitation," vol. 129, no. 8, pp. 1036-1046, 2003.

[20] H. Takizawa, P. C. J. E. E. Jennings, and S. Dynamics, "Collapse of a model for ductile reinforced concrete frames under extreme earthquake motions," vol. 8, no. 2, pp. 117-144, 1980.

[21] F. Zareian, H. Krawinkler, L. Ibarra, D. J. T. S. D. o. T. Lignos, and S. Buildings, "Basic concepts and performance measures in prediction of collapse of buildings under earthquake ground motions," vol. 19, no. 1-2, pp. 167-181, 2010.

[22] R. A. Medina, R. Sankaranarayanan, and K. M. J. E. s. Kingston, "Floor response spectra for light components mounted on regular moment-resisting frame structures," vol. 28, no. 14, pp. 1927-1940, 2006.

[23] D. Vamvatsikos and C. A. Cornell, "The incremental dynamic analysis and its application to performance-based earthquake engineering," in *Proceedings of the 12th European conference on earthquake engineering*, 2002, vol. 40: Citeseer.

[24] F. Zareian, H. J. E. E. Krawinkler, and S. Dynamics, "Assessment of probability of collapse and design for collapse safety," vol. 36, no. 13, pp. 1901-1914, 2007.

[25] S. A. Ahamad and K. J. M. T. P. Pratap, "Dynamic analysis of G+ 20 multi storied building by using shear walls in various locations for different seismic zones by using Etabs," 2020.

[26] J. Seo, J. W. Hu, and B. Davaajamts, "Seismic performance evaluation of multistory reinforced concrete moment resisting frame structure with shear walls," *Sustainability,* vol. 7, no. 10, pp. 14287-14308, 2015.

[27] A. Coull and Y. Wong, "Effect of local elastic wall deformations on the interaction between floor slabs and flanged shear walls," *Building and Environment,* vol. 20, no. 3, pp. 169-179, 1985.

[28] P. Hidalgo, R. Jordan, and M. Martinez, "An analytical model to predict the inelastic seismic behavior of shear-wall, reinforced concrete structures," *Engineering Structures,* vol. 24, no. 1, pp. 85-98, 2002.

[29] A. Tasnimi, "Strength and deformation of mid-rise shear walls under load reversal," *Engineering Structures,* vol. 22, no. 4, pp. 311-322, 2000.

[30] B. Burak and H. G. Comlekoglu, "Effect of shear wall area to floor area ratio on the seismic behavior of reinforced concrete buildings," *Journal of Structural Engineering,* vol. 139, no. 11, pp. 1928-1937, 2013.

[31] F. Dashti, R. P. Dhakal, and S. Pampanin, "Comparative in-plane pushover response of a typical RC rectangular wall designed by different standards," *Earthq. Struct,* vol. 7, no. 5, pp. 667-689, 2014.

[32] P. Heerema, M. Shedid, D. Konstantinidis, and W. El-Dakhakhni, "System-level seismic performance assessment of an asymmetrical reinforced concrete block shear wall building," *Journal of Structural Engineering,* vol. 141, no. 12, p. 04015047, 2015.

[33] O. A. El-Azizy, M. T. Shedid, W. W. El-Dakhakhni, and R. G. Drysdale, "Experimental evaluation of the seismic performance of reinforced concrete

structural walls with different end configurations," *Engineering Structures*, vol. 101, pp. 246-263, 2015.

[34] A. Gogus and J. W. Wallace, "Seismic safety evaluation of reinforced concrete walls through FEMA P695 methodology," *Journal of Structural Engineering*, vol. 141, no. 10, p. 04015002, 2015.

[35] A. Guide, A. Manual, and A. RP, "ACI 318, Building Code Requirements for Structural Concrete (ACI 318-05) and Commentary (ACI 318R-05), ACI Committee 318, American Concrete Institute, Farmington Hills, MI, 2005 ACI 530, Building Code Requirements for Masonry Structures (ACI 530-05/ASCE 5-05/TMS 402-05), American Concrete Institute, Farmington Hills, MI, 2005."

[36] B. Li, Z. Pan, and W. Xiang, "Experimental evaluation of seismic performance of squat RC structural walls with limited ductility reinforcing details," *Journal of Earthquake Engineering*, vol. 19, no. 2, pp. 313-331, 2015.

[37] M. Khanmohammadi and S. Heydari, "Seismic behavior improvement of reinforced concrete shear wall buildings using multiple rocking systems," *Engineering Structures,* vol. 100, pp. 577-589, 2015.

[38] A. Jalali and F. Dashti, "Nonlinear behavior of reinforced concrete shear walls using macroscopic and microscopic models," *Engineering Structures,* vol. 32, no. 9, pp. 2959-2968, 2010.

[39] Y. D. Aktaş, "Seismic resistance of traditional timber-frame hımış structures in Turkey: A brief overview," *International Wood Products Journal,* vol. 8, no. sup1, pp. 21-28, 2017.

[40] M. O. Sanni-Anibire, M. A. Hassanain, and A.-M. Al-Hammad, "Post-occupancy evaluation of housing facilities: Overview and summary of methods," *Journal of Performance of Constructed Facilities,* vol. 30, no. 5, p. 04016009, 2016.

[41] J. Ji, A. S. Elnashai, and D. Kuchma, "Seismic fragility assessment for reinforced concrete high-rise buildings," *MAE Center CD Release 07-14*, 2007.

[42] W. Alwaeli, A. Mwafy, K. Pilakoutas, and M. Guadagnini, "Framework for developing fragility relations of high-rise RC wall buildings based on verified modelling approach," in *The Proceedings of the Second European Conference on Earthquake Engineering and Seismology*, 2014.

[43] Z. T. Değer, T. Y. Yang, J. W. Wallace, and J. Moehle, "Seismic performance of reinforced concrete core wall buildings with and without moment resisting frames," *The Structural Design of Tall and Special Buildings,* vol. 24, no. 7, pp. 477-490, 2015.

[44] Z. T. Değer and J. W. Wallace, "Seismic performance of reinforced concrete dual-system buildings designed using two different design methods," *The structural design of tall and special buildings,* vol. 25, no. 1, pp. 45-59, 2016.

[45] M. Aman, H. Nadeem, and E. S. Khaled, "Seismic performance and cost-effectiveness of high-rise buildings with increasing concrete strength," *The Structural Design of Tall and Special Buildings,* vol. 24, no. 4, pp. 257-279, 2015.

[46] E. S. Firoozabad, K. R. M. Rao, and B. Bagheri, "Effect of shear wall configuration on seismic performance of building," in *International Conference on Advances in Civil Engineering*, 2012, pp. 121-125: Citeseer.

[47] A. Chandiwala, "Earthquake analysis of building configuration with different position of shear wall," *International Journal of Emerging Technology and Advanced Engineering,* vol. 2, no. 12, pp. 347-353, 2012.

[48] S. J. Sardar and U. N. Karadi, "Effect of change in shear wall location on storey drift of multi Storey building subjected to lateral loads," *International Journal of Innovative Research in Science Engineering and Technology,* vol. 2, no. 9, 2013.

[49] J. Kim, J. Lee, and S. Han, "Seismic performance of building structures with spatial variability," *International Journal of Engineering and Technology,* vol. 5, no. 6, p. 721, 2013.

[50] E. Sanaei and M. Babaei, "Topology optimization of structures using cellular automata with constant strain triangles," *International Journal of Civil Engineering,* vol. 10, no. 3, pp. 179-188, 2012.

[51] M. H. R. Sobuz *et al.*, "Performance assessment of various seismic resistant systems for a multistory structure in different seismic zones of Bangladesh," *Journal of Engineering, Design and Technology,* 2022.

[52] J. G. YADAV and P. RAJESH, "SEISMIC BEHAVIOUR OF RC BUILDING CONSTRUCTRED WITH DIFFERENT CONFIGURATIONS OF SHEAR WALLS."

[53] ASCE-7-22, "Minimum Design Loads and Associated Criteria for Buildings and Other Structures," *American Society of Civil Engineers: Reston, VA, USA, 2022.*, 2022.